(2)

ARMY RESEARCH LABORATORY

ARL

Anti-Tank Spike-Nosed Projectiles With Vortex Rings: Steady and Non-Steady Flow Simulations

Ameer G. Mikhail

ARL-TR-101 March 1993

NOTICES

Destroy this report when it is no longer needed. DO NOT return it to the originator.

Additional copies of this report may be obtained from the National Technical Information Service, U.S. Department of Commerce, 5285 Port Royal Road, Springfield, VA 22161.

The findings of this report are not to be construed as an official Department of the Army position, unless so designated by other authorized documents.

The use of trade names or manufacturers' names in this report does not constitute indorsement of any commercial product.

REPORT DOCUMENTATION PAGE

Form Approved
OMB No. 0704-0188

1. AGENCY USE ONLY (Leave blank)	2. REPORT DATE	3. REPORT TYPE AND DATES COVERED
	March 1993	Final, January 1990 - January 1991

4. TITLE AND SUBTITLE

ANTI-TANK SPIKE-NOSED PROJECTILES WITH VORTEX RINGS: STEADY AND NON-STEADY FLOW SIMULATIONS

5. FUNDING NUMBERS

1L162618AH80
62618A-00-001 AJ

6. AUTHOR(S)

AMEER G. MIKHAIL

7. PERFORMING ORGANIZATION NAME(S) AND ADDRESS(ES)

U. S. Army Research Laboratory
ATTN: AMSRL-WT-PB
Aberdeen Proving Ground, MD 21005-5066

8. PERFORMING ORGANIZATION REPORT NUMBER

9. SPONSORING/MONITORING AGENCY NAME(S) AND ADDRESS(ES)

US Army Research Laboratory
ATTN: AMSRL-OP-CI-B (Tech Lib)
Aberdeen Proving Ground, Maryland 21005-5066

10. SPONSORING/MONITORING AGENCY REPORT NUMBER

ARL-TR-101

11. SUPPLEMENTARY NOTES

This report supersedes BRL-IMR-962, dated April 1991.

12a. DISTRIBUTION/AVAILABILITY STATEMENT

Approved for public release; distribution is unlimited.

12b. DISTRIBUTION CODE

13. ABSTRACT (Maximum 200 words)

Numerical computations are reported for a spike-nosed projectile configuration with a vortex generator ring. A new vortex-dominated flow field is computed at supersonic speeds of M = 3.5, 3.0, and 1.9. A time-dependent Navier-Stokes computational technique with a zonal gridding was used. The axial force at zero angle of attack was computed and found to be in good agreement with the wind tunnel data at Mach 3.0. The sting quantitative effect on the axial force coefficient and the flow pattern was found to be very minor for the present case at Mach 3.5. A high drag solution for a case computed at Mach 3.5 was obtained by imposing a cross flow velocity of seven percent of the freestream velocity. This result removed any doubt that the wind tunnel results for that Mach number were for the high drag mode. An additional interesting case was computed at Mach 1.9; and the flow was found to be of the oscillatory (buzzing) type. The frequency of the oscillation was computed as 5333 Hz and indicated that the designers of the projectile in 1980 were apparently not aware of the possible buzzing flow along the projectile trajectory when it decelerates from Mach 3.5 to 1.9. They had tested the projectile only at Mach 3.5 and 3.0. No tests were made at Mach 1.9 or lower.

14. SUBJECT TERMS

Anti-Tank Projectiles	Spikes	Aerodynamic Drag
Supersonic Drag	Numerical Integration	Axisymmetric Flow
Turbulent Flow	Flow Field	Unsteady Flow

15. NUMBER OF PAGES

44

16. PRICE CODE

17. SECURITY CLASSIFICATION OF REPORT	18. SECURITY CLASSIFICATION OF THIS PAGE	19. SECURITY CLASSIFICATION OF ABSTRACT	20. LIMITATION OF ABSTRACT
UNCLASSIFIED	UNCLASSIFIED	UNCLASSIFIED	UL

INTENTIONALLY LEFT BLANK.

Table of Contents

INTENTIONALLY LEFT BLANK.

List of Figures

INTENTIONALLY LEFT BLANK.

I. INTRODUCTION

Spike-nosed projectile configurations are used against armored targets where the spike provides a stand-off distance between the armor and the shaped-charge warhead. These projectiles have been continuously developed and improved, despite their high drag disadvantage. One major difficulty with the spike-nosed configurations is the possibility of two flow patterns. In many cases, one does not know which flow pattern will occur under what conditions. One flow pattern is of low drag and the other is of a higher drag. Unfortunately, the high drag pattern is more dominant and more stable while the lower drag pattern is less dominant and occurs in fewer cases. Some projectiles launched at high supersonic speeds start with the high drag and then switch to the lower drag mode which is more stable at a lower speed. In other cases the flow may oscillate slowly between the two modes. In other configurations the flow oscillates rapidly causing the "buzzing" phenomenon. The critical Mach number for switching patterns depends on the Mach number, length of the spike, spike diameter to projectile diameter ratio, and to a lesser degree on the Reynolds number and flow turbulence.

Platou[1] reported the two flow patterns experienced during supersonic wind tunnel testing in the early 1950's. Koenig et al[2] more recently reported hysteresis mode changes during transonic wind tunnel testing. Shang and Hankey[3] successfully and accurately simulated the buzzing phenomenon in the 1970's for a re-entry body with a relatively short spike. Calarese and Hankey[4] tested and analyzed the oscillations of spike-tipped bodies. Mikhail[5] in 1989 successfully computed the flow past three sharp-edged, spike-nosed configurations and induced the two modes for each case. Mikhail verified his results at Mach = 1.72 with those wind tunnel tests of Reference 1.

To avoid the uncertainity of the dual flow modes, it had been found long ago that by inserting a ring near the spike tip the high drag mode is prevented by introducing flow separation along the spike and preventing reattachment before the flow faces the projectile shoulder which causes a shoulder "bow" shock and the high drag. No specific name is credited in the literature for suggesting such a "tripping" device. This ring device should more appropriately be named "vortex generator" ring due to its major effect on creating a new vortex-dominated flow field, rather than to its effect on "creating separation". The usual notion of "tripping", induced from the laminar to turbulent boundary layer tripping devices, is wrong. However, its use, unfortunately, is wide spread among researchers.

The present study concerns itself with projectiles with "tripping" rings of interest to the U.S. Army. In particular, the interest is drawn from the 105 mm M489 spike-nosed projectile. This round is the training round for the 105 mm M456A1 fin-stabilized, High Explosive Anti-Tank (HEAT) projectile. Computations at three different Mach numbers are performed and the sting support effect is studied to assess its influence. The results are compared with wind tunnel data for verification. A new and interesting flow pattern was observed and is described. Also, for a high drag case, the high drag solution was induced by a technique described earlier in Reference 5. Further, a "buzzing" flow case was encountered and the frequency of buzzing was computed.

II. PROJECTILE GEOMETRY AND THE TEST CASES

The projectile configuration of interest to the U.S. Army is the 105 mm M490 spin-stabilized projectile of the M489 training round. Wind tunnel test results were available from Reference 6 at only two Mach numbers: 3.0 and 3.5. The wind tunnel models were of 2.0-inch diameter which represent only 48% of the full scale projectile. Several variations in the projectile spike diameter, projectile shoulder geometry, and the afterbody were tested. The chosen configuration for the present study was model number 1112, which is depicted in Figure 1. The tests were run in a blow-down supersonic wind tunnel with the following test conditions: Mach numbers (3.0,3.5), total pressure (60.0,70.0) psi, total temperature (59.0,59.0) $^{\circ}F$, and Reynolds number (10.2,9.1) $\times 10^6$ per foot, respectively. Some range firing tests were also made for the spinning full scale projectile[7]. However, due to the yawing motion observed and lack of documentation, the zero yaw axial force coefficient was not readily available. Also it should be noted that the scaling laws between the full scale and the 0.48 scaled models for spike-nosed bodies are not known. The flow pattern and the flow over the spike are highly sensitive to the spike length (in association with the local Reynolds number influencing the separation region along the spike) and in conjunction with the projectile shoulder diameter (the shoulder diameter to the spike diameter ratio). Therefore, the wind tunnel results were favored for the numerical simulation.

The sting support was 0.67 inch in diameter, corresponding to 0.333 of the model base diameter. Cases of angles of attack between $\pm 8^{\circ}$ were tested and measured. No error bounds on any of the given measurements were given in the report of Reference 6.

III. COMPUTATIONAL TECHNIQUE

1. GOVERNING EQUATIONS

The compressible, turbulent Navier-Stokes equations for axisymmetric and two-dimensional flow can be expressed[8] in the following strong conservation form where the dependent variables ρ, u, v, and e are mass averaged where e being the specific total energy, u and v are the axial and radial velocity components, ρ and p being mean density and pressure, respectively, and t is time:

$$\frac{\partial Q'}{\partial t} + \frac{\partial E'}{\partial x} + \frac{\partial F'}{\partial y} + \left(\frac{F'}{y} + \frac{H'}{y}\right)\beta = 0$$

where

$$Q' = \begin{bmatrix} \rho \\ \rho u \\ \rho v \\ \rho e \end{bmatrix} \quad E' = \begin{bmatrix} \rho u \\ \rho u u + p - \tau_{xx} \\ \rho u v - \tau_{xy} \\ (\rho e + p)u - \tau_{xx}u - \tau_{xy}v + \dot{q}_x \end{bmatrix}$$

$$F' = \begin{bmatrix} \rho v \\ \rho uv - \tau_{xy} \\ \rho vv + p - \tau_{yy} \\ (\rho e + p)v - \tau_{xy}u - \tau_{yy}v + \dot{q}_y \end{bmatrix} \quad H' = \begin{bmatrix} 0 \\ 0 \\ -p + \sigma_+ \\ 0 \end{bmatrix}$$

$$\tau_{xx} = -\frac{2}{3}(\mu + \epsilon)\tilde{\nabla} \cdot \tilde{V} + 2(\mu + \epsilon)\frac{\partial u}{\partial x}$$

$$\tau_{xy} = (\mu + \epsilon)\left(\frac{\partial u}{\partial y} + \frac{\partial v}{\partial x}\right)$$

$$\tau_{yy} = -\frac{2}{3}(\mu + \epsilon)\tilde{\nabla} \cdot \tilde{V} + 2(\mu + \epsilon)\frac{\partial v}{\partial y}$$

$$\tau_{\Theta\Theta} = \sigma_+ = -\frac{2}{3}(\mu + \epsilon)\tilde{\nabla} \cdot \tilde{V} + 2(\mu + \epsilon)\frac{v}{y}$$

$$\tilde{\nabla} \cdot \tilde{V} = \frac{\partial u}{\partial x} + \frac{\partial v}{\partial y} + \left(\frac{v}{y}\right)\beta$$

$$\dot{q}_x = -C_p\left(\frac{\mu}{Pr} + \frac{\epsilon}{Pr_t}\right)\frac{\partial T}{\partial x}$$

$$\dot{q}_y = -C_p\left(\frac{\mu}{Pr} + \frac{\epsilon}{Pr_t}\right)\frac{\partial T}{\partial y} \qquad (1)$$

where μ is the molecular viscosity and ϵ is eddy viscosity and $\beta = 1$ or 0 for axisymmetric and two-dimensional cases, respectively.

The air is assumed to be perfect gas, satisfying the equation of state

$$p = \rho RT$$

where R is the gas constant ($1716 ft^2/sec^2\text{-}R^0$ for air). For the dependence of laminar viscosity on temperature, Sutherland's law was used:

$$\mu = 2.270\frac{T^{3/2}}{T + 198.6} \times 10^{-8} \quad \frac{lb - sec}{ft^2}.$$

The laminar and turbulent Prandtl numbers, Pr and Pr_t, were assumed constant with values of 0.72 and 0.9 respectively. The ratio of the specific heats, γ, was also assumed constant and equal to 1.4. C_v and C_p are specific heat capacities at constant volume and constant pressure, respectively.

$$C_v = 4290 \frac{ft^2}{sec^2 - R^0}$$

and

$$C_p = 6006 \frac{ft^2}{sec^2 - R^0}$$

for air. The total energy per unit mass, e, is given by:

$$e = C_v T + (1/2)(u^2 + v^2).$$

In the $\xi - \eta$ computational plane, Equation 1 is transformed to the conservation law form and the equations can be found, for example, in Reference 8.

2. TURBULENCE MODEL

Turbulence is modeled through a modification to the eddy viscosity model of Baldwin and Lomax[9]. This widely applied model employs the two-layer concept (inner and outer layers). The inner layer is near the wall and is modeled as:

$$\epsilon_i = \rho l^2 |\omega| \tag{2}$$

$$l = ky \left[1 - exp\left(\frac{-y^+}{A^+} \right) \right] \tag{3}$$

The magnitude of the vorticity $|\omega|$ is:

$$|\omega| = |\frac{\partial u}{\partial y} - \frac{\partial v}{\partial x}| \tag{4}$$

and where

$$y^+ = \left(\frac{\rho_w |\omega_w|}{\mu_w} \right)^{1/2} y \tag{5}$$

The distance normal to the surface is y, $A^+ = 26$, $k = 0.40$ is the von Karman constant, and the subscript w denotes values at the surface.

The model switches from the inner to the outer region at the smallest value of y which the inner and outer values of the eddy viscosity are equal (i.e, $\epsilon_i = \epsilon_o$). The ϵ for the outer layer is given by:

$$\epsilon_o = \rho K C_{cp} F_{max} y_{max} F_{KLEB} \tag{6}$$

where

$$F_{max} = y_{max}|\omega| \left[1 - exp\left(\frac{-y^+}{A^+}\right)\right]. \tag{7}$$

The value of y at which F_{max} occurs is y_{max}.

$$F_{KLEB} = \left[1 + 5.5\left(\frac{C_{KLEB} \times y}{y_{max}}\right)^6\right]^{-1} \tag{8}$$

$$K = 0.0168, \qquad C_{cp} = 1.6, \qquad C_{KLEB} = 0.3. \tag{9}$$

Due to the perpendicular intersection of the spike surfaces at the nose tip and also at the facing shoulder, the normal distance to these walls "y" in Equations 2-8 is difficult to assign[10]. This problem was approached in Reference 10 by measuring the y along a 45° ray emanating from the point of intersection of the two perpendicular walls.

3. THE CODE

The computer code was developed by Patel et al[8] and utilizes the robust explicit, time dependent method of McCormack. The code is vectorized and is run on Cray-XMP/48 machine. However the present computations were all run in serial arithmetic mode. The zonal grid and overlapping is provided in the code as represented by eight different zones (can be increased if so desired). The user prescribes the overlapping between regions along one line of adjacent zones (interface). A global uniform time step was used herein rather than grid-varying time steps to simulate "time-accurate" solutions. The time step is determined from the CFL (Courant-Fredrich-Levy) condition, with a factor of 0.6 being used as the Courant number. One characteristic time length for the flow field at M =3.0 and 3.5 was 454. $\times 10^{-6}$ and 389. $\times 10^{-6}$ second, respectively. With an average time step of 0.19 $\times 10^{-6}$ sec, one characteristic time length corresponds to 2390 and 2050 numerical time steps at Mach = 3.0 and 3.5 , respectively .

4. BOUNDARY CONDITIONS

No-slip conditions are specified on all wall surfaces. The incoming flow conditions are assumed to be of uniform profiles with freestream values based on the wind tunnel test values.

M_∞	$T_\infty(R°)$	$P_\infty(psi)$	$Re(per\,ft)$
1.9	302	7.31	12.62×10^6
3.0	185	1.63	10.20×10^6
3.5	150	0.98	9.10×10^6

The outgoing flow conditions at the downstream end of the flow field were imposed as zero gradients along the body axis direction at a distance of 4.0 body diameters behind the projectile base.

The outer boundary conditions were imposed as non reflective conditions, i.e.. zero gradient conditions along characteristic lines for all variables. The characteristic direction is determined from the local velocity and temperature. This approach allows setting the "outer" field close to the body without the penalty of any unnecessary approximation regarding shock reflection, or degradation due to far-field conditions (no-gradients) being set too close .

At the symmetry line, ahead of the spike tip and behind the base, a two-point zero gradient boundary condition is imposed on the solved variables.

5. INITIAL CONDITIONS

Computations for the first case of Mach 3.0 were started using free stream values everywhere in the domain for all variables, based on an initial lower Mach number which was selected as 1.5. These values are for free stream pressure, and temperature. The density and specific total energy are computed accordingly, using the equation of state and the definition of the specific total energy. The rest of the cases were started in the same manner except for the case of Mach 3.5 with no sting, which was started using the solution for the case with the sting at the same Mach number.

6. THE GRID

Six different grid zones were used in the computation. Those zones and the extent of the computational domain are depicted in Figure 2.

For the case with a sting, the grid used for the six zones are (20,85), (13,72), (7,65), (60,78), (130,36), and (80,31) respectively. The first and second arguments in the brackets refer to the axial and radial directions, respectively. This grid is equivalent to 16531 total points or about a (129x129) grid. For the case of no sting, the same grid is used except the last zone which was increased from (80x31) to (80x51) to account for the space previously occupied by the sting.

One restriction in the present grid overlapping technique is that no interpolation is allowed at the interface line between zones. Thus, each point on either side of any two zones must have the exact same coordinates. This restriction represents some constraint in the flexibility of the grid distribution and may be alleviated in future development of the code. Meanwhile, to accommodate this restriction one has to accept unnecessary clustering of points in some locations. Figures 3 and 4 show the overall grid distribution for the projectile configuration with and without sting, respectively. Figure 5 shows the details of the grid near the spike, depicting the clustered points along lines parallel to the top body surface where clustering is needed near the body to resolve the turbulent boundary layer.

IV. RESULTS

1. THE CASE AT M = 3.0

This case was started using the earlier stated initial conditions and the previously described grid with the sting. A new flow field, dominated by the vortex and wake generated by the "tripping" ring, extended over the projectile middle body and beyond the base of the projectile. This vortex-wake stream interfered with the usual expansion wave expected at the base for the supersonic flow. The wake flow eliminated the expansion wave and the "outer" supersonic flow slipped over the wake stream almost unturned thus, no expansion wave took place. At first, this behavior was suspect but was later confirmed when the spark shadowgraph photos for the corresponding full scale projectile (obtained during the range test firing of Reference 7) were reviewed. Examination of the shadowgraphs immediately confirmed the computations and showed little trace of the expected expansion wave. In addition, the shadowgraph showed very clearly the vortex-wake region emanating from the vortex ring and flowing all the way over the projectile body. This flow field, now appearing to be logical and acceptable was, nevertheless, not expected. This is the first time in the known literature that such particular flow field has been analyzed and computed. A schematic of the flow pattern is shown in Figure 6 and is compared with the typical expected flow for a spiked body without a tripping ring. This vortex-dominated field effect on the expansion wave at the base was never shown in the literature and was not exposed in Mikhail's work[5] since no base region computations were made for the spiked configurations with a tripping ring.

The flow field is depicted in Figures 7-9 by the Mach-line contours for the regions near the spike tip, the shoulder, and the base of the projectile. The axial force coefficient, here also is the drag coefficient, was computed to be 0.253 which compares extremely well with the value of 0.255 of the wind tunnel data[6]. This drag comparison is depicted in Figure 10.

The case took about 40,000 time steps to converge only because there is a very small eddy continuously breaking down and reforming near the base and which propagates upwind to the frontal spike tip. It is not known at this point whether this unsteadiness is truely physical or purely numerical in nature. This caused the drag coefficient to vary slightly at a very slow frequency. The drag coefficient variation is provided in Figure 11 as a drag history plot.

Figure 12 provides the anatomy of the drag for the case at M = 3.0, showing the value of each component of the drag. The shoulder drag was 47%, while the base pressure drag was 18% of the total drag. The spike frontal area caused 30% of the total drag, while the skin friction of the whole body contributed a mere 0.2%. The vortex ring contributed only 4.4%.

The computation time on the Cray XMP/48 was about 40 minutes for each 1000 time steps. For a 40,000 steps this amounts to about 27 hours of CPU time.

2. THE CASE AT M = 3.5

The case with the sting was started from the same uniform initial conditions described earlier. The case took about 58,000 steps to converge with this high number being due, as explained above, to the small eddy break-up. The computations could have been stopped at half the number of steps with no appreciable difference. However, it was kept running to: first, observe any changes; and second, to ensure that no numerical instability would occur.

The axial force coefficient computed was 0.233 which, as expected, is lower than the value for the $M = 3.0$ case. However, the tunnel test provided a higher value of $C_D = 0.309$. It was immediately realized that the tunnel test resulted in the high-drag value while the computation resulted in the low-drag flow pattern value. Also, the sting was suspected to influence the frontal spike flow pattern through this oscillating small structure eddy. Therefore, the effect of the sting had first to be assessed.

a. Effect of the Sting

The sting was removed and the new grid replacing the space previously occupied by the sting was constructed. The new grid is depicted in Figure 4. The solution was started from the point where the case with a sting ended. The computations did not take more than 10,000 steps to settle again and converge. Surprisingly, no appreciable difference was observed in the frontal spike flow or in the flow pattern. Only changes in the base flow were observed, as expected. Two eddies near the base disappeared when the sting was removed. The new C_D value obtained was 0.232 compared to the 0.233 for the case with the sting. The small eddy break-up also existed. The flow field for the case with and without sting is given in Figures 13-14.

b. The High Drag Case

With the computed axial force coefficient being lower than the wind tunnel value, the need to compute the corresponding high drag case was necessary. Based on the prior experience cited in Reference 5, the high drag mode was then "induced" by the method cited which suggested a pseudo simulation of the effect of an angle of attack. For the present case, a cross flow velocity of 0.07 of the freestream velocity value was imposed as a boundary condition for the incoming flow (a pseudo 4-degree yaw as described in Reference 5). The sting was put back for the simulation of the existing wind tunnel case. The computations were started from the previous solution of $M = 3.5$ case with a sting.

The computation took 30,000 steps to converge (20 hours CPU time). The computed C_D was 0.347. This value obtained falls between the scatter of the two wind tunnel data points of 0.309 and 0.386. The latter value was for an identical projectile which was one inch shorter in the body length (near the base of the projectile) than the present configuration.

The flow fields for both the low and high-drag cases are very similar except at the base near the sting. The flow fields are depicted in Figures 15-16. Figure 17 shows the drag coefficient comparison with the wind tunnel measurement. The numerical convergence

history is given in Figure 18.

3. THE CASE AT M = 1.9

After the computations of the above two cases, the variation of C_D with the Mach number was of interest due to the low- and high- drag cases encountered at the $M = 3.5$ case. Although no wind tunnel data is available at lower speeds, an additional case at $M = 1.9$ was chosen for computation to assess the C_D variation with Mach number for this particular projectile configuration. Having no wind tunnel data to compare with, and after the previous result that the sting had no effect on the spike flow, the $M = 1.9$ case with no sting was computed to simulate the in-flight behavior of the projectile.

The computation started from the same uniform initial conditions and, after a large number of time steps, the solution showed a very clear type of oscillatory (buzzing) behavior. This buzzing is of a different class than the small unsteadiness observed earlier due to the small eddy break-up. The clear oscillatory behavior was observed to be cyclic after about 80,000 steps and persisted to 110,000 steps with a very constant frequency of about 3000 steps per cycle. Therefore, ten complete cycles were encountered before the computations were stopped. This buzzing flow pattern had no equal amplitude in the pressure oscillation, attributable to the non-cyclic eddy break-up. This same phenomenon is frequently observed in combustor flow applications, with and without combustion processes. For example Jou and Menon[11] in their study of non reacting flow inside a ramjet combustor, obtained a buzzing flow with a variable pressure amplitude due to the large eddies existing in the flow past the sudden expansion section. The flow in their case oscillated cyclically with a favored frequency but with variable pressure amplitude. The same phenomenon there was also explained as the effect of continuous formation and break-up of large eddies in the flow.

For the present case, with the time step $\Delta t = 0.19 \times 10^{-6}$ sec, the frequency of the buzz was 5333 Hz. The drag coefficient oscillated between about 0.22 and 0.62 with a "mean" value of about 0.42. The flow pulsated between high pressure and low pressure points. The oscillatory drag behavior is depicted in Figure 19 and the more detailed oscillatory cycle is shown in Figure 20. The unequal amplitude of the oscillation was disturbing at first, but when consulting the literature, the same behavior was readily confirmed. Jou and Menon[11]obtained a large eddy break-up pattern when computing non-reacting flow in a dump combustor. The flow in their case also oscillated with non-equal amplitude.

The flow field for this interesting buzzing flow is captured both at the high and low pressure points of the cycle. Figures 21-26 depict the flow near the spike tip, the shoulder, and the projectile base. Some flow changes are observed as the flow pulsates very rapidly.

Finally, the drag coefficient variation with the Mach number is depicted in Figure 27 for all cases computed and is compared with the available wind tunnel data. The data validates the computations at Mach 3.0 and 3.5, while the computations extend the results down to Mach 1.9.

V. SUMMARY AND CONCLUSIONS

Five computations were made for a spike-nosed projectile with a vortex ring at Mach 1.9, 3.0, and 3.5 at zero angle of attack. The computations were made by solving Navier-Stokes equations in an overlapped zonal gridding topology, using McCormack's explicit scheme. The results obtained are summarized as follows:

1. A new flow pattern which is dominated by the vortex and wake generated by the "tripping" ring is computed and described . The vortex-wake field extends to the base of the projectile and interfers with the usual flow expansion there. This flow was verified by very clear firing range spark shadowgraph photos for the full scale model tests[7]. The axial force coefficient was in excellent agreement with the wind tunnel data at Mach 3.0.

2. At Mach 3.5, both low and high drag patterns were obtained. The high drag value agrees with the wind tunnel data. This experimental data was reported[6] without explanation of why the drag was higher at Mach 3.5 than at Mach 3.0.

3. The sting effect on the flow pattern and axial force was studied and found to be almost non-existent for the present sting diameter which was only 0.33 of the projectile diameter. The base flow pattern, however, was influenced and showed at least two eddies, which vanished when the sting was removed, for the case of Mach 3.5.

4. A detailed drag anatomy was provided , shedding a very interesting light onto the total drag picture of the projectile. The front spike contributed 30%, while the "shoulder" drag is 47% of the total drag for the case at Mach 3.0.

5. At the lower Mach number of 1.9, the interesting "buzzing" (unsteady) flow was encountered and was computed successfully. The frequency of oscillation was found to be 5333 Hz. The axial force coefficient oscillated between 0.22 and 0.62, with a "mean" value of 0.42. No wind tunnel tests were done at that Mach number. Therefore, the designers of the projectile were apparently not aware of the possible buzzing flow at lower Mach numbers.

The numerical procedure proved to be robust and reliable once "enough" grid points are used. The computations proceeded in a straight forward manner and without major interruptions, adding to the previous success reported in Reference 5 for spike-nosed bodies. Possible future improvements should consider better turbulence model for the base region, as well as more thorough modeling for turbulence in the recirculating flow region ahead of the projectile shoulder.

Finally, it is recommended to further test the present numerical procedure on more complex spike-nosed configurations, such as for those with fin boom, boattail, and fins. Efforts are currently being made to follow up on this recommendation.

WIND TUNNEL MODEL FOR THE 105 MM M490 TRAINING HEAT PROJECTILE

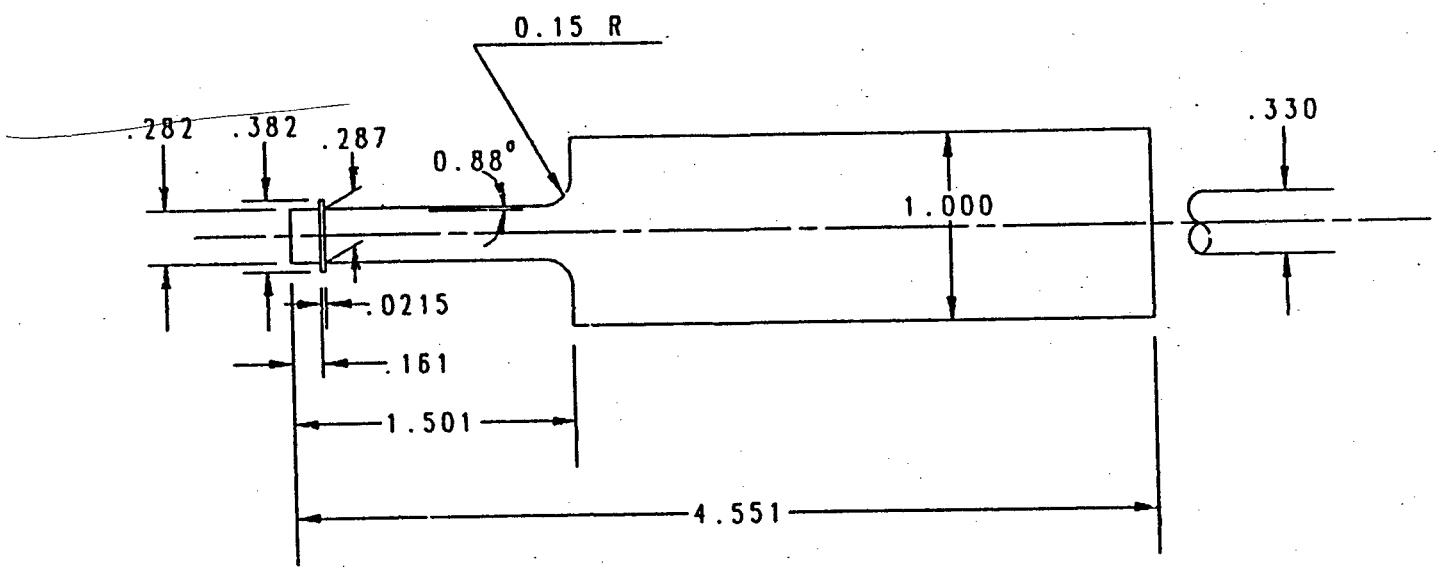

DIMENSIONS IN CALIBERS
1 CALIBER = 2.002 INCHES (50.85 MM)

Figure 1. Projectile wind tunnel model configuration

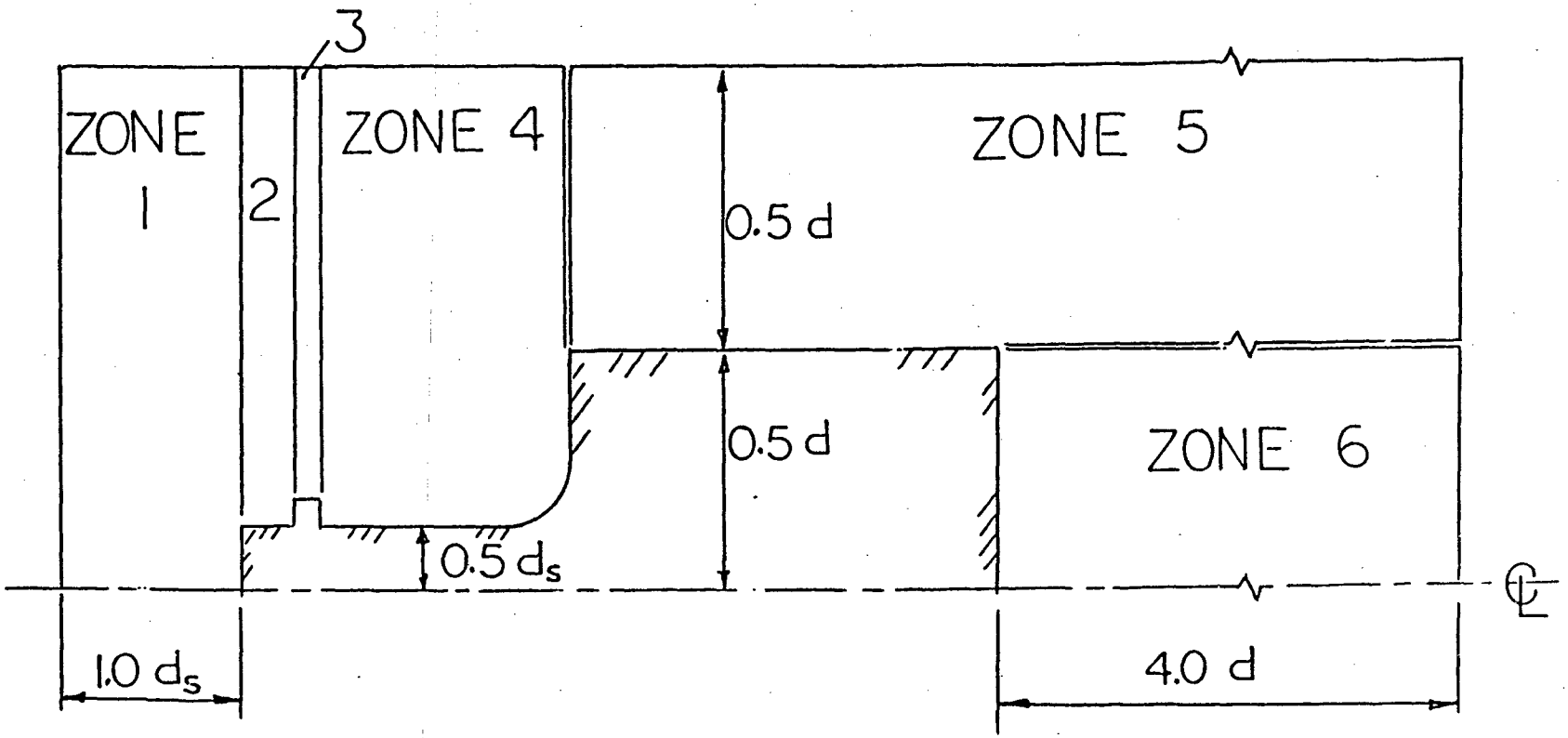

Figure 2. Grid zones and computational domain

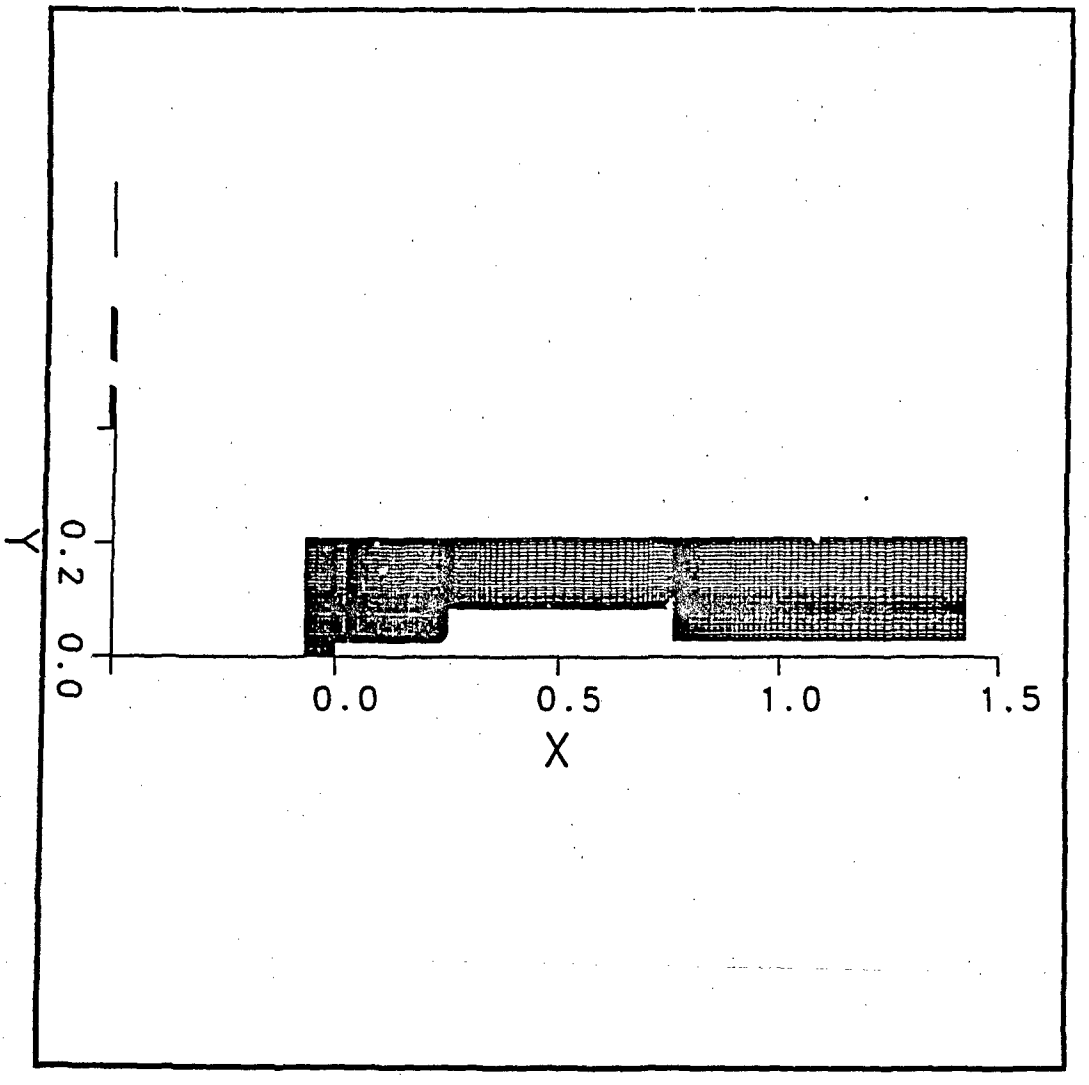

Figure 3. Computational grid case - with a sting support

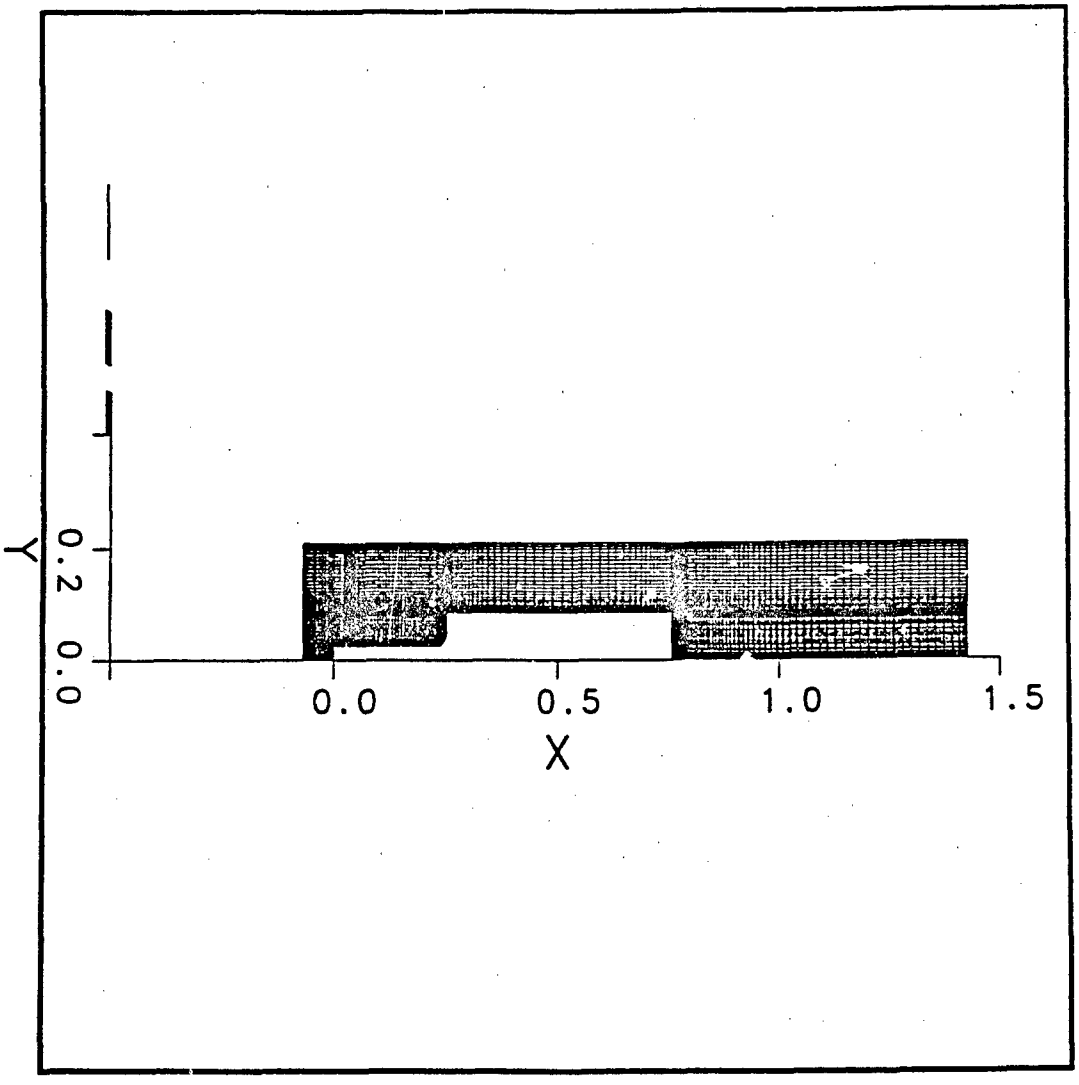

Figure 4. Computational grid case - with no sting

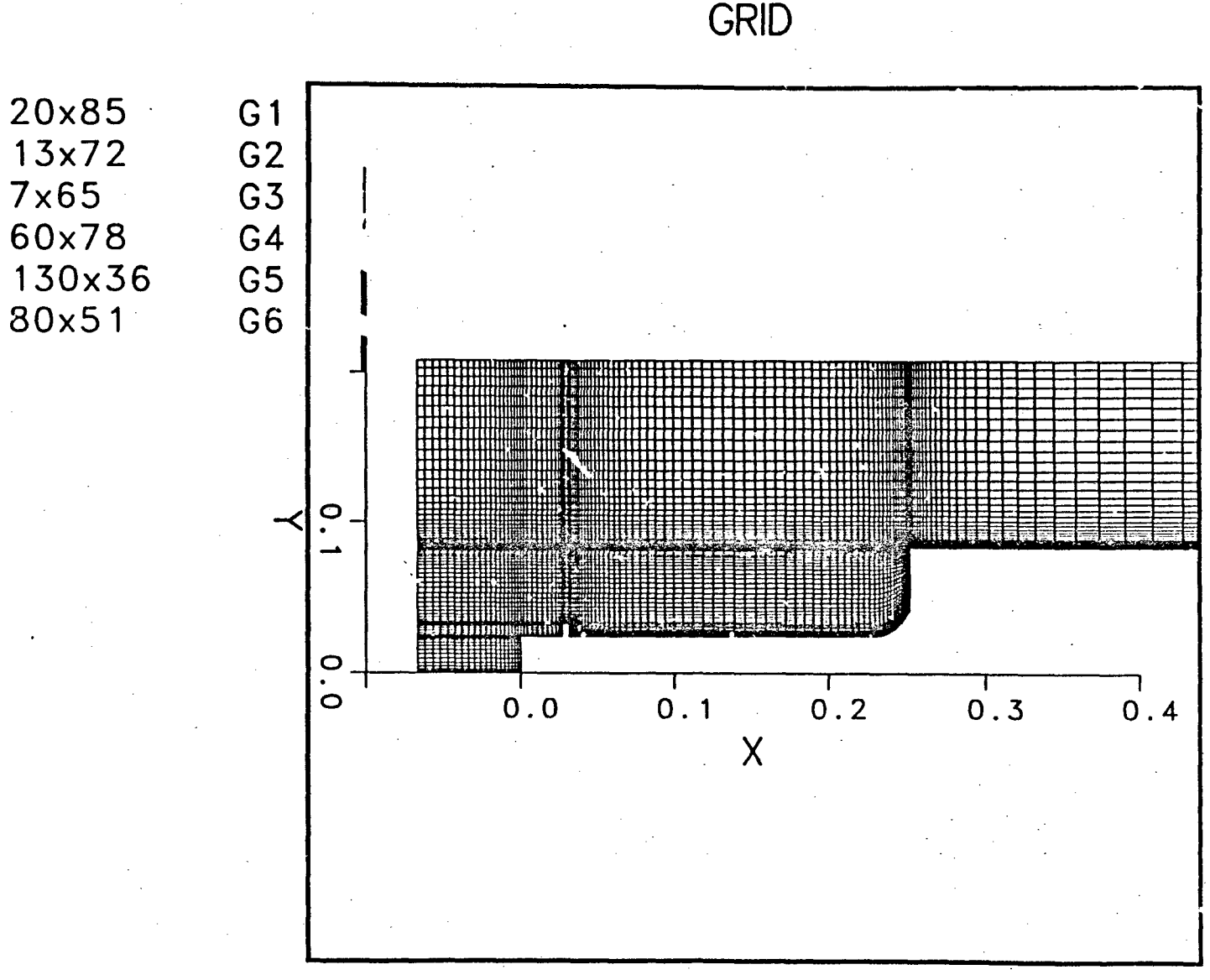

Figure 5. Details of the grid near the spike

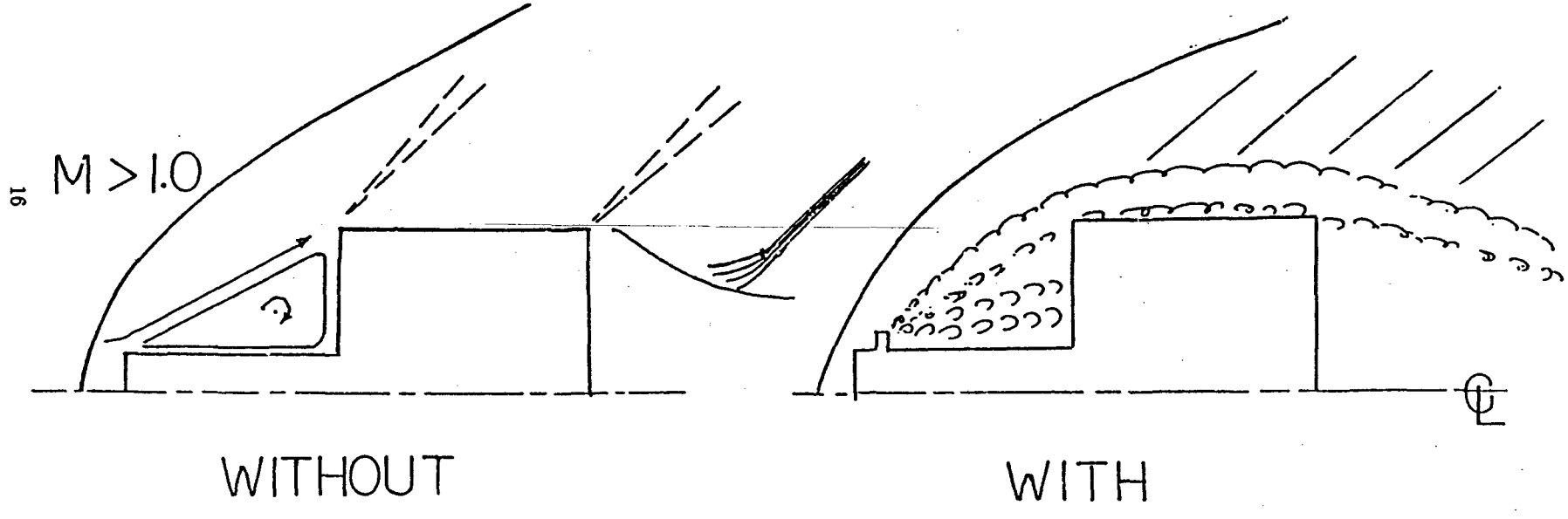

Figure 6. Flow patterns for spiked projectiles with and without a tripping ring

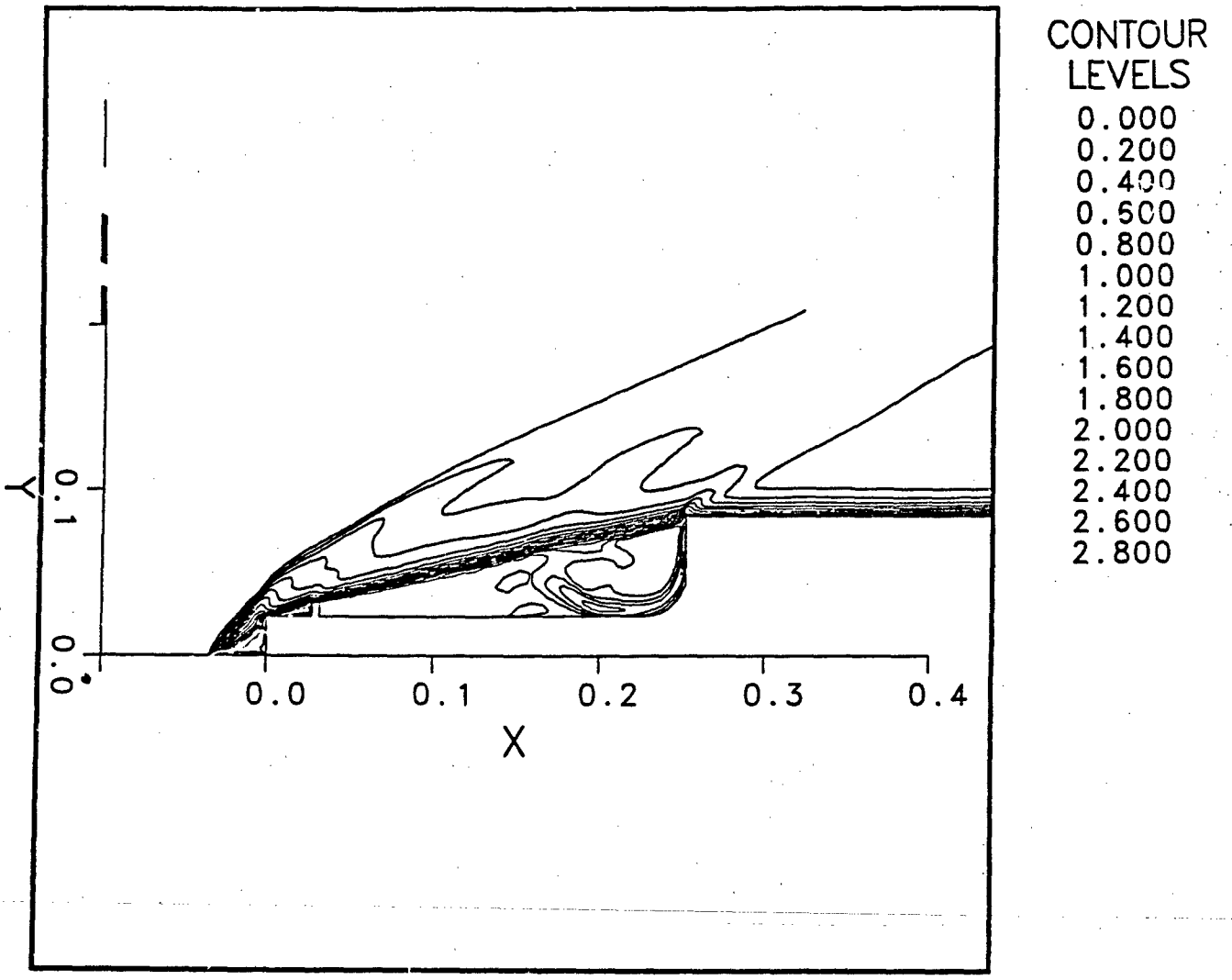

Figure 7. Flow field for M = 3.0 case - Mach-line contours near the spike tip

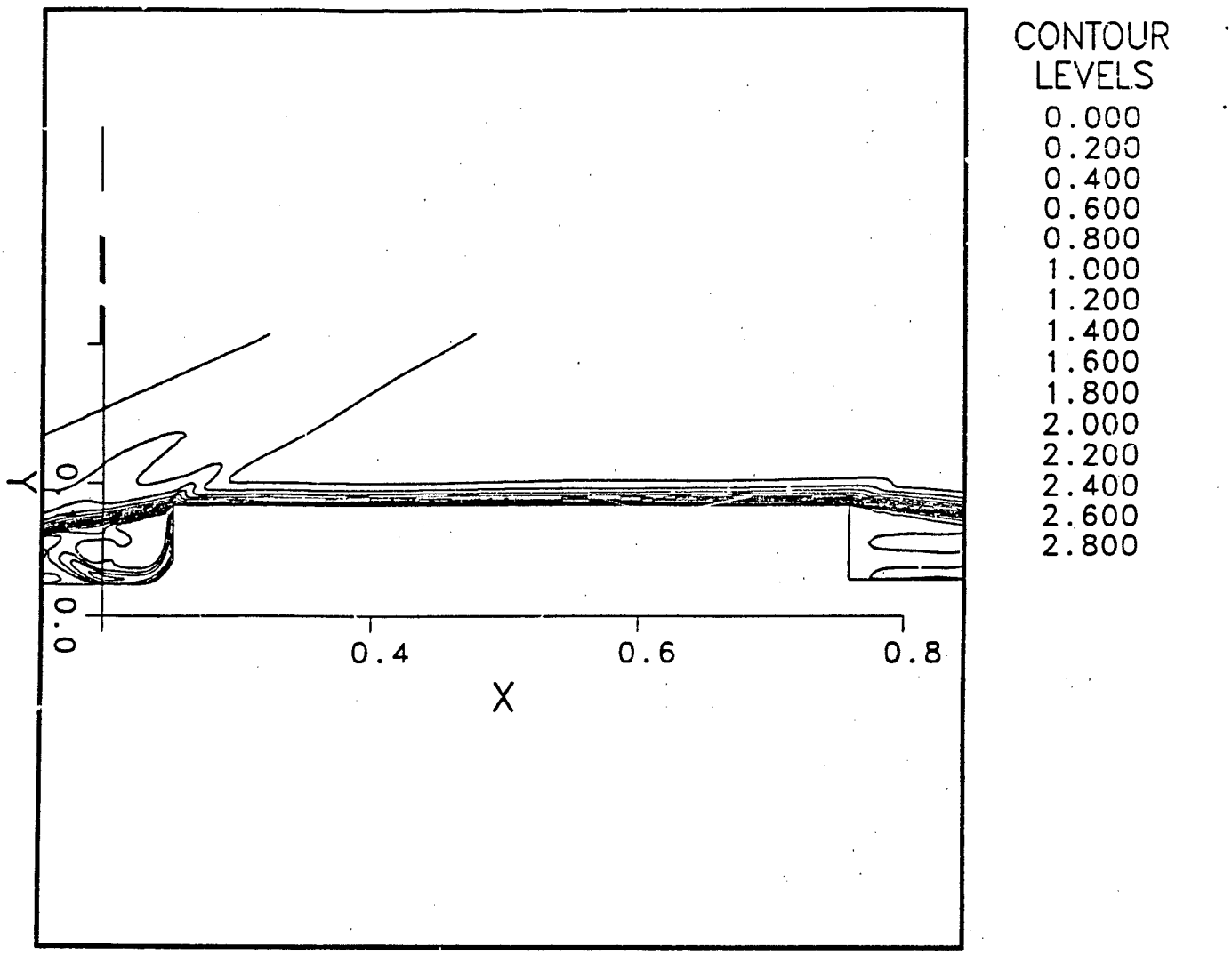

Figure 8. Flow field for M = 3.0 case - Mach-line contours near projectile shoulder

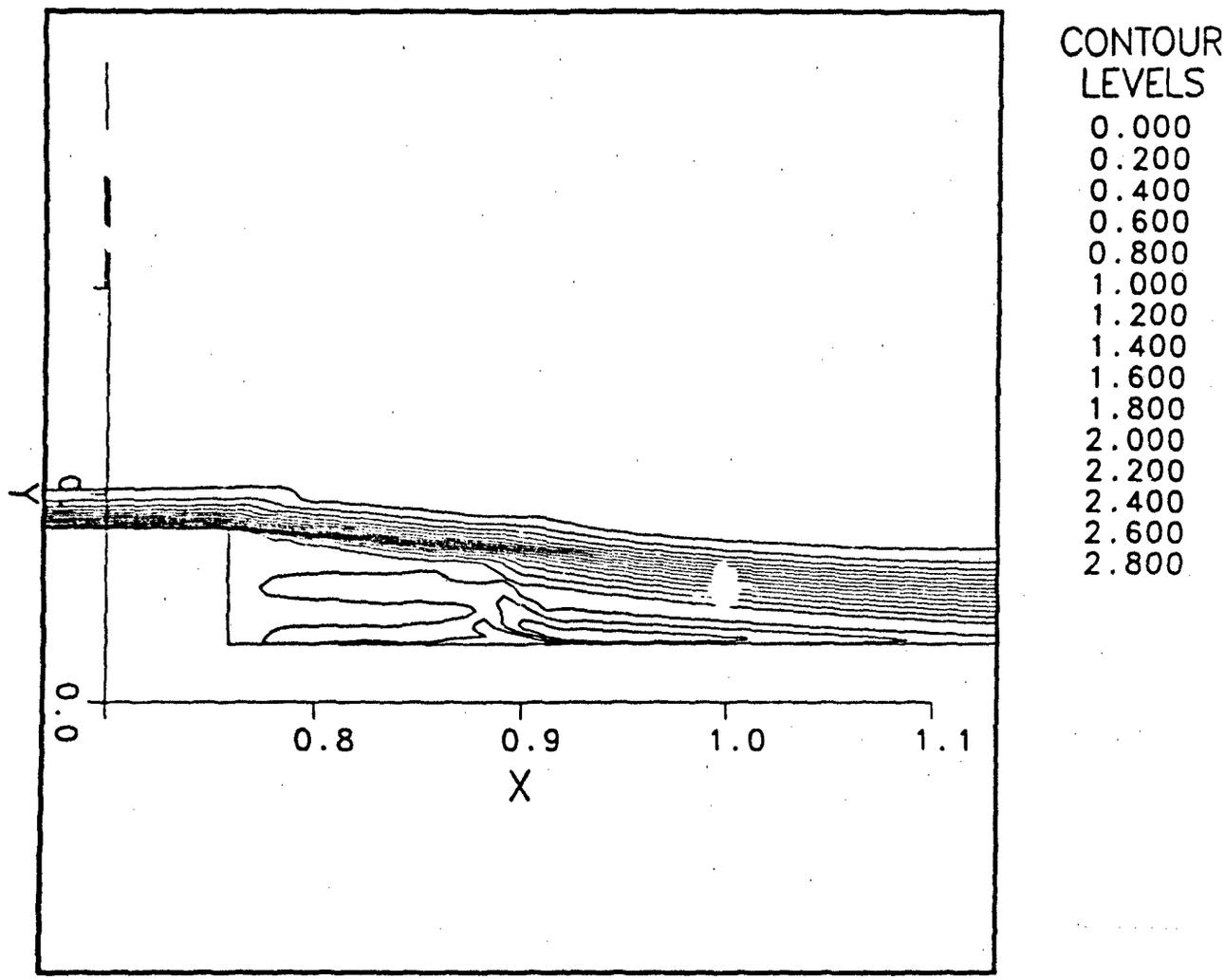

Figure 9. Flow field for M = 3.0 case - Mach-line contours near the sting support

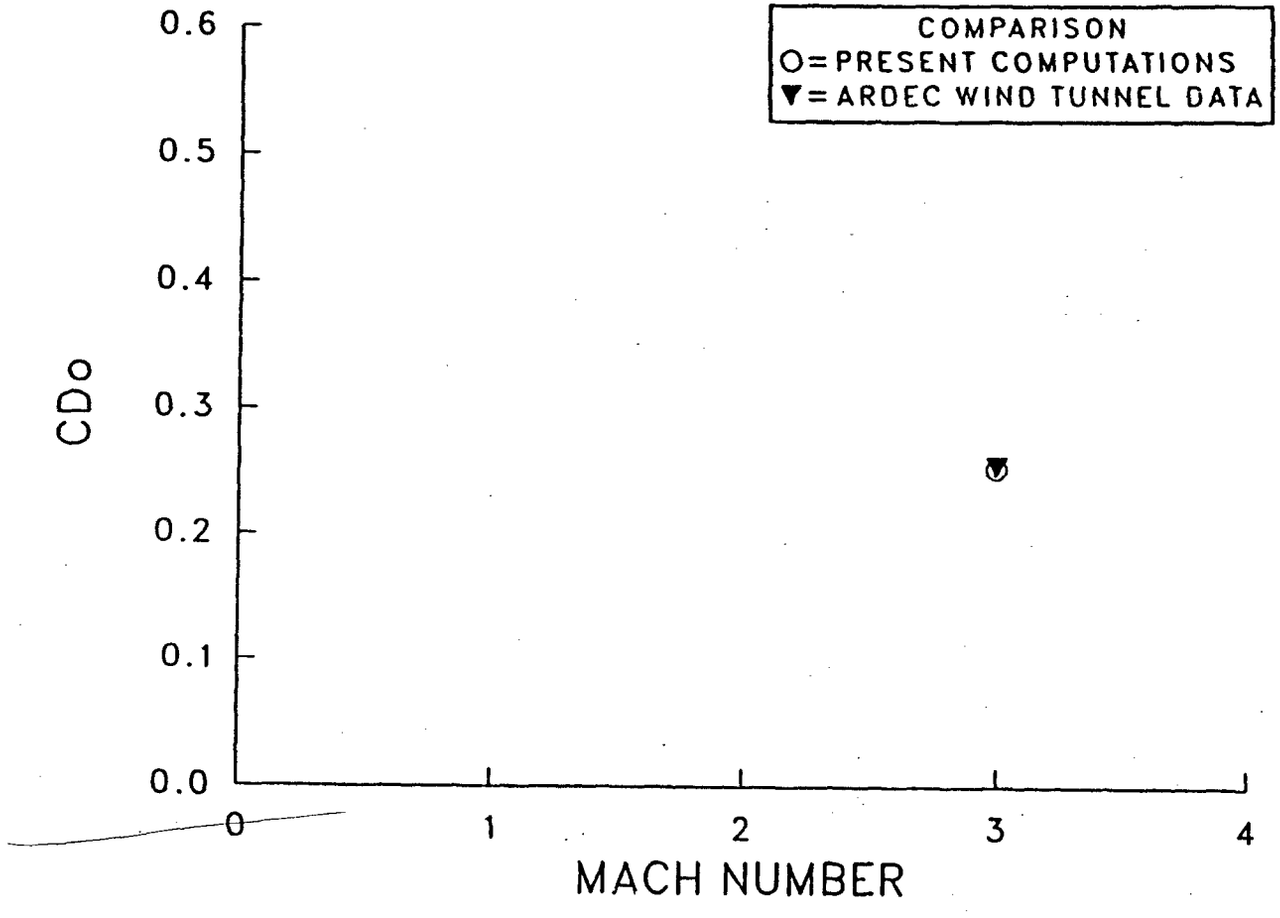

Figure 10. Drag coefficient comparison for M = 3.0 case

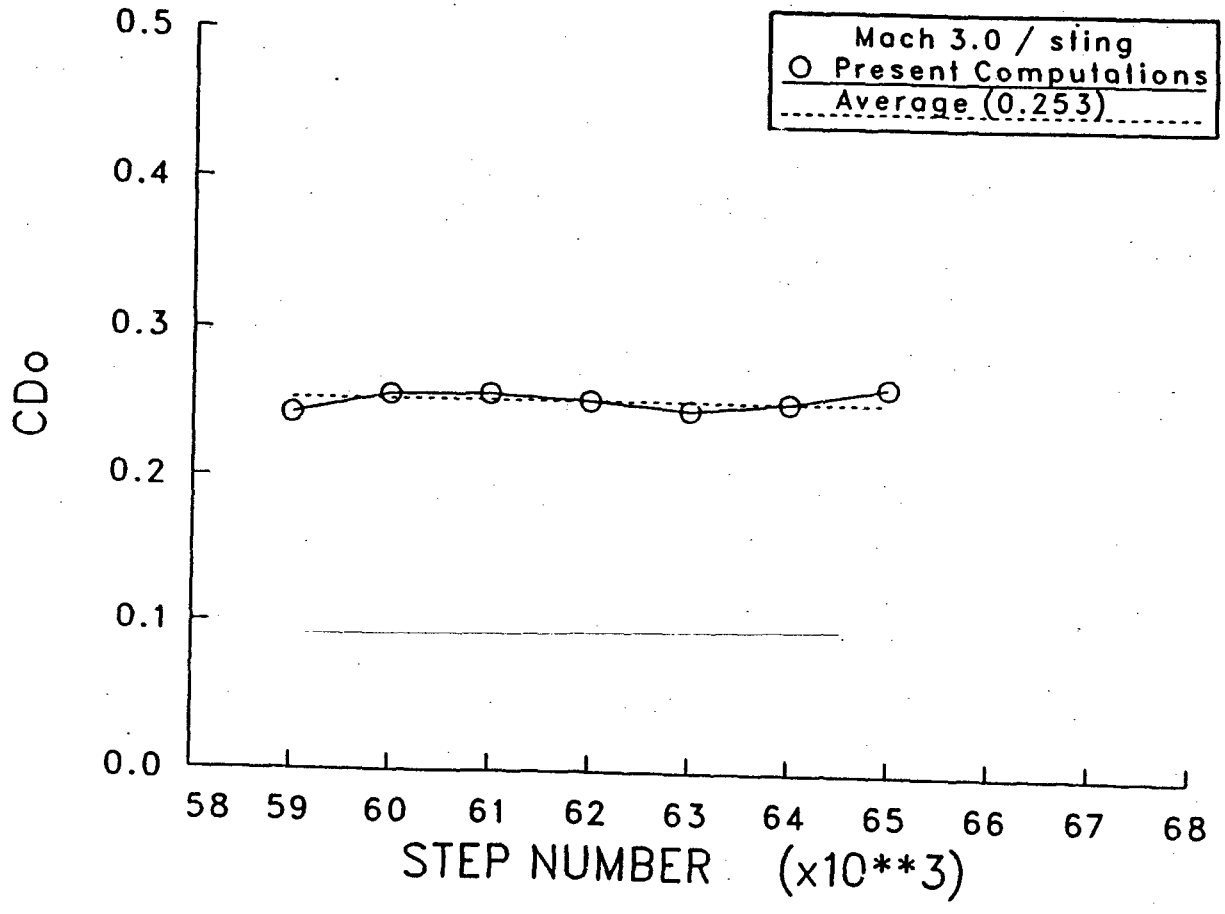

Figure 11. Numerical conversion history for M = 3.0 case

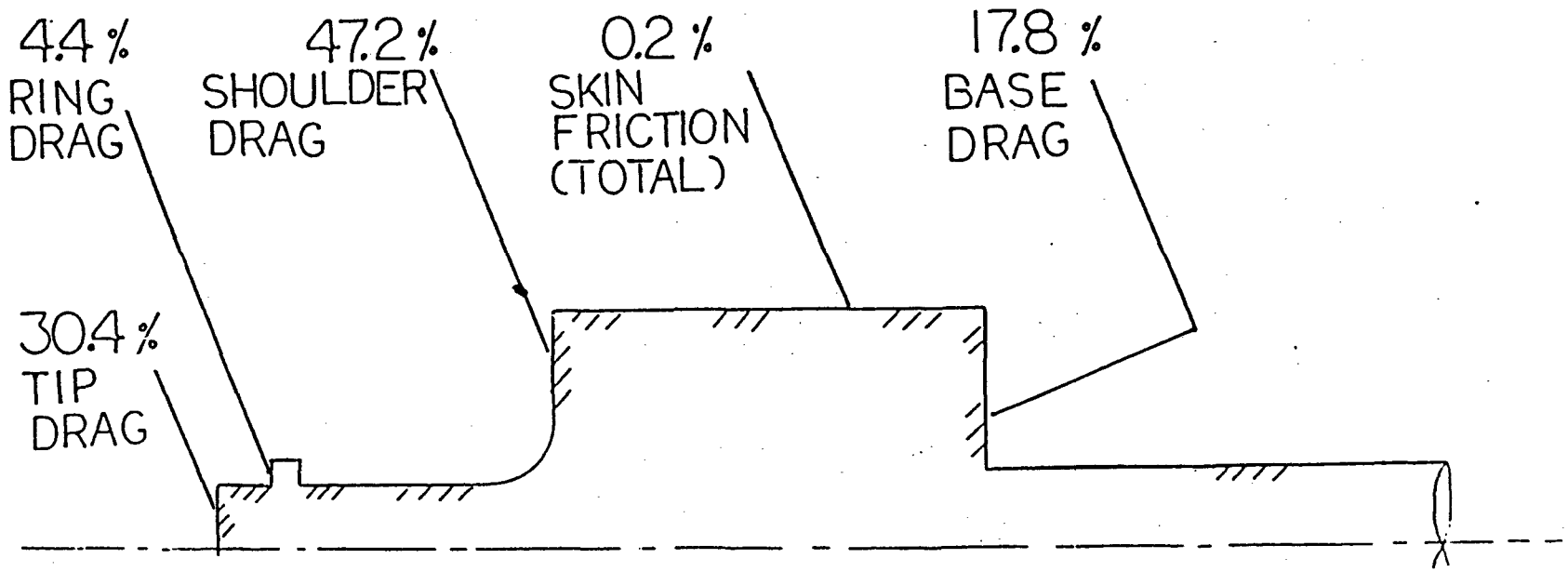

Figure 12. Drag anatomy for M = 3.0 case

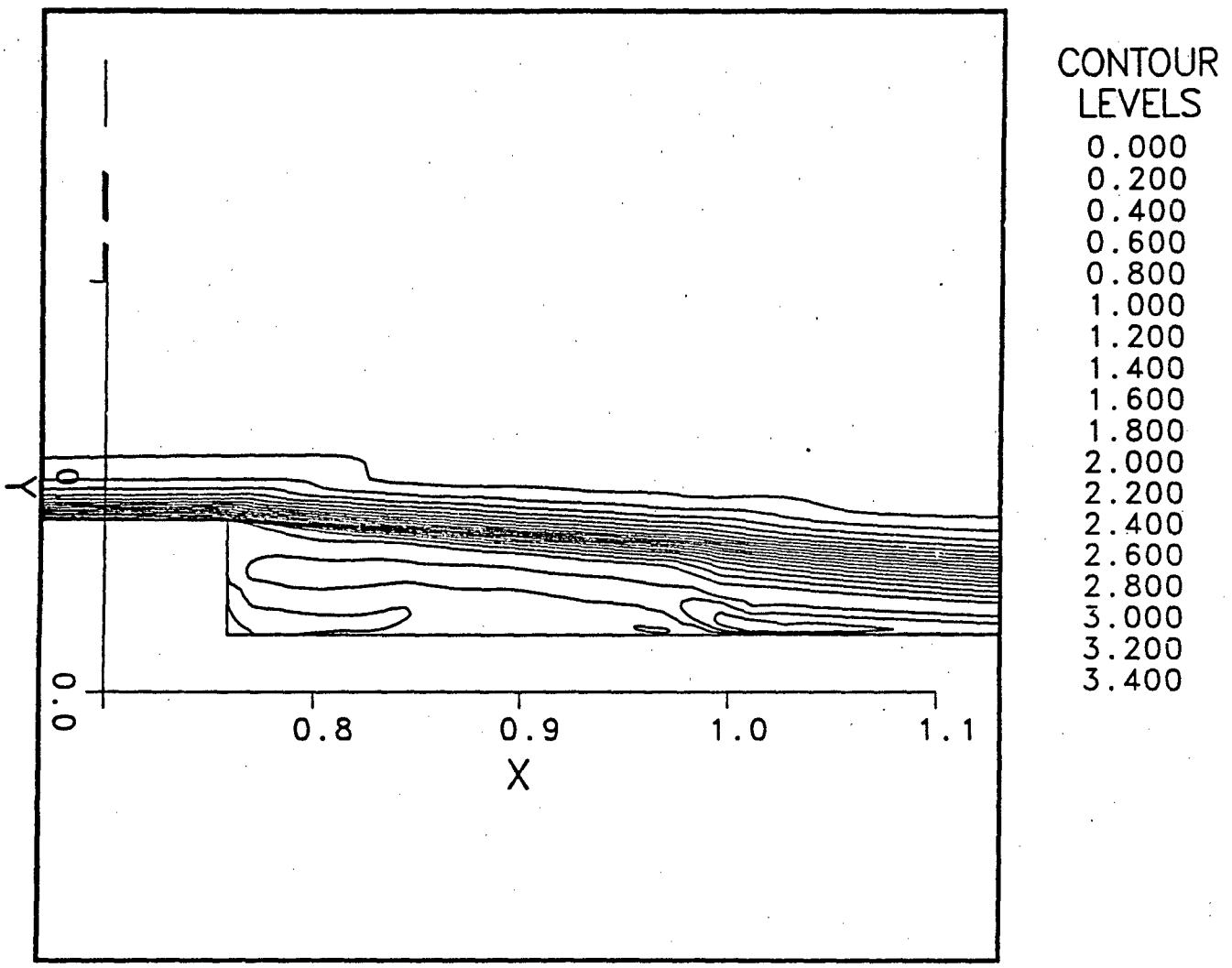

Figure 13. Flow field for M = 3.5 case - Mach-line contours for case with sting

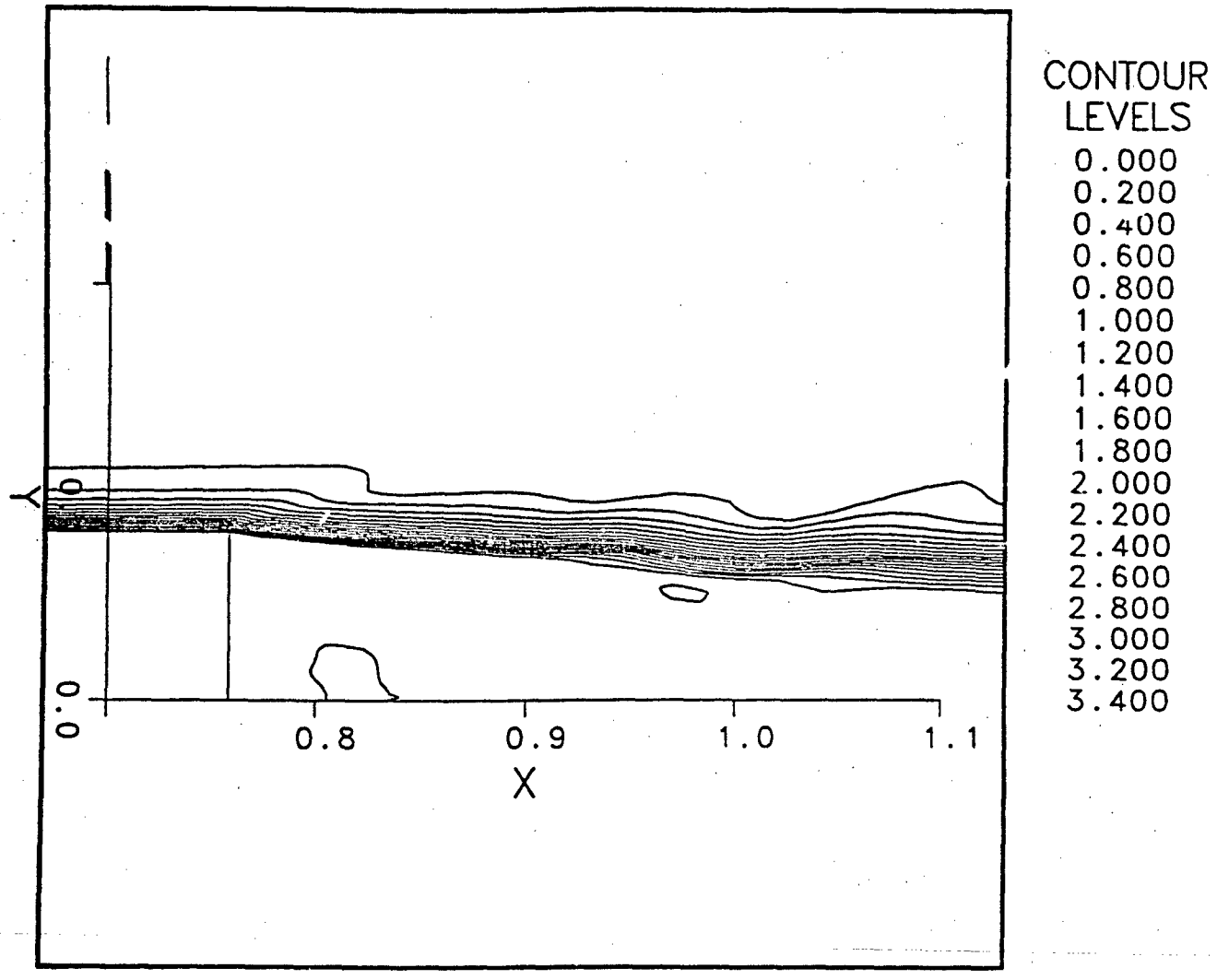

Figure 14. Flow field for M = 3.5 case - Mach-line contours for case without sting

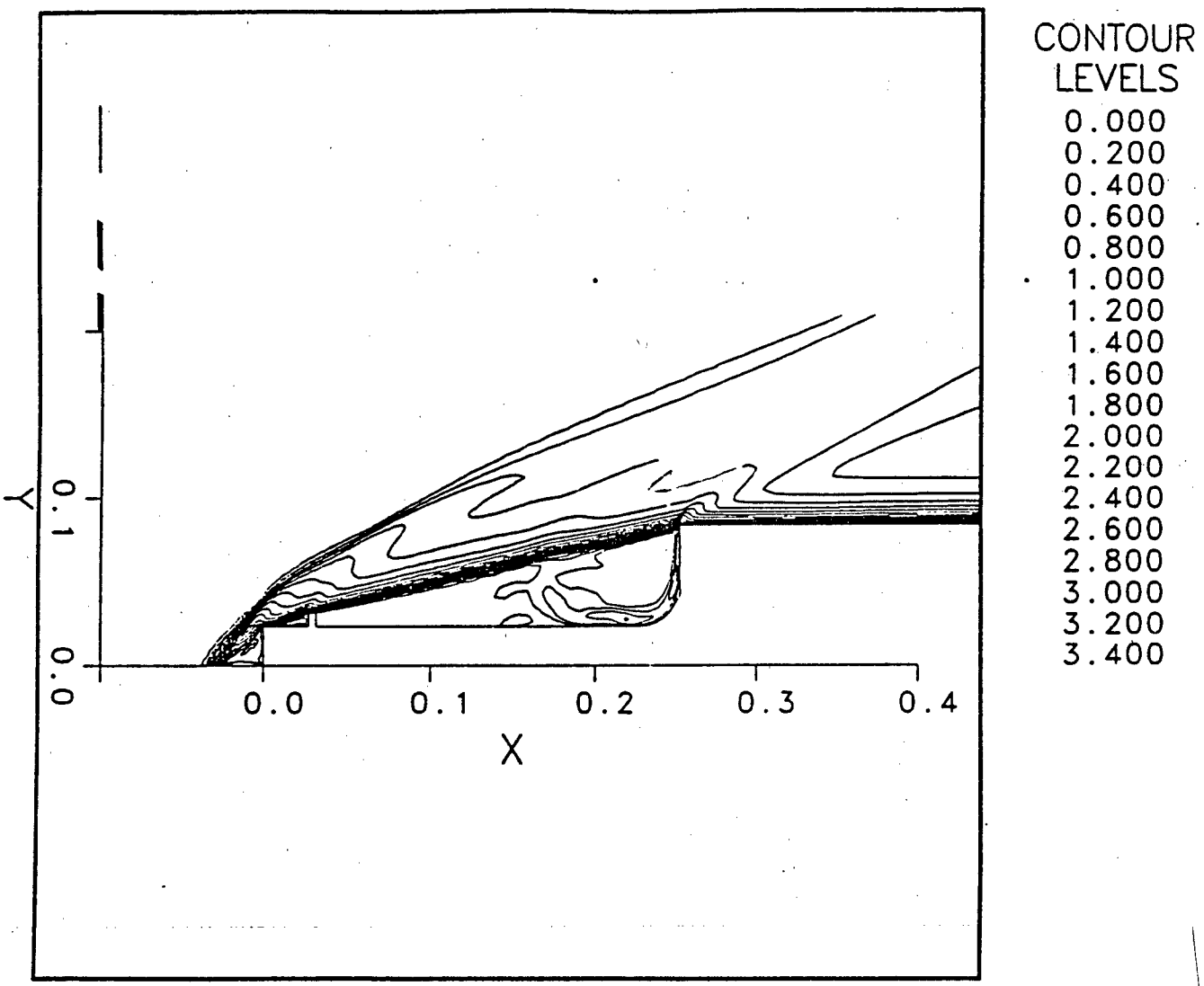

Figure 15. Flow field for M = 3.5 case - Mach-line contours for the low-drag pattern

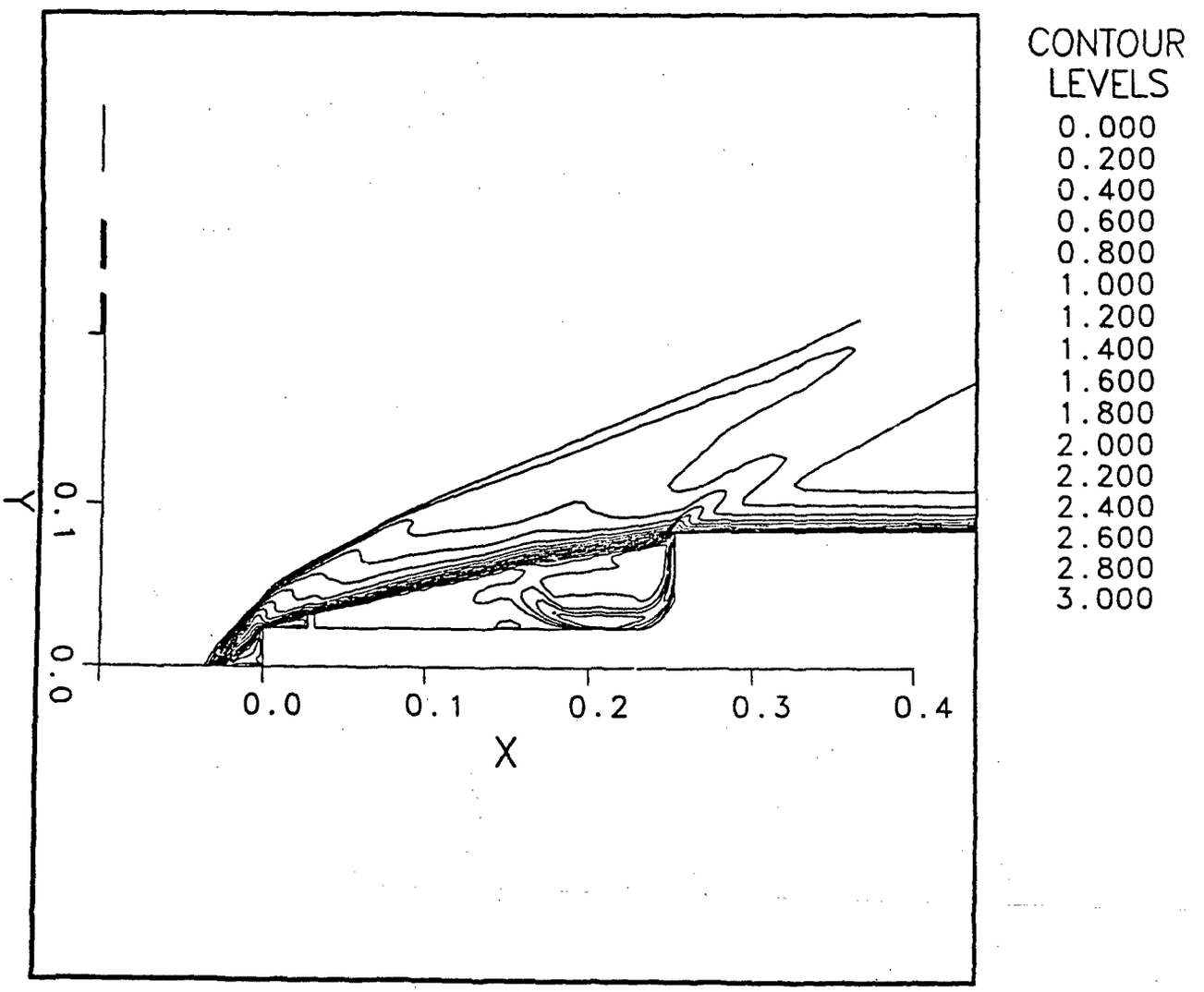

Figure 16. Flow field for M = 3.5 case - Mach-line contours for the high-drag pattern

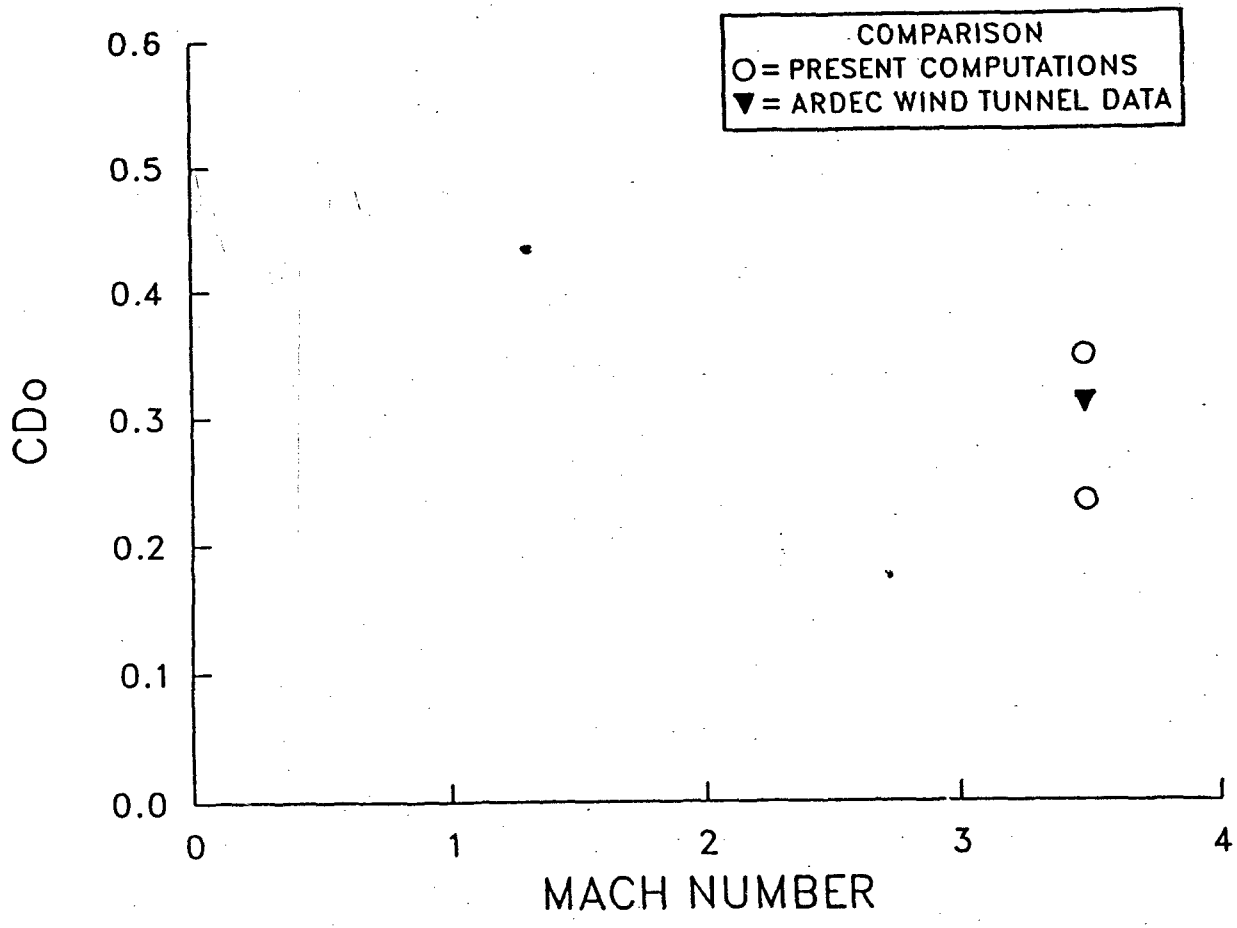

Figure 17. Drag coefficient comparison for M = 3.5 case

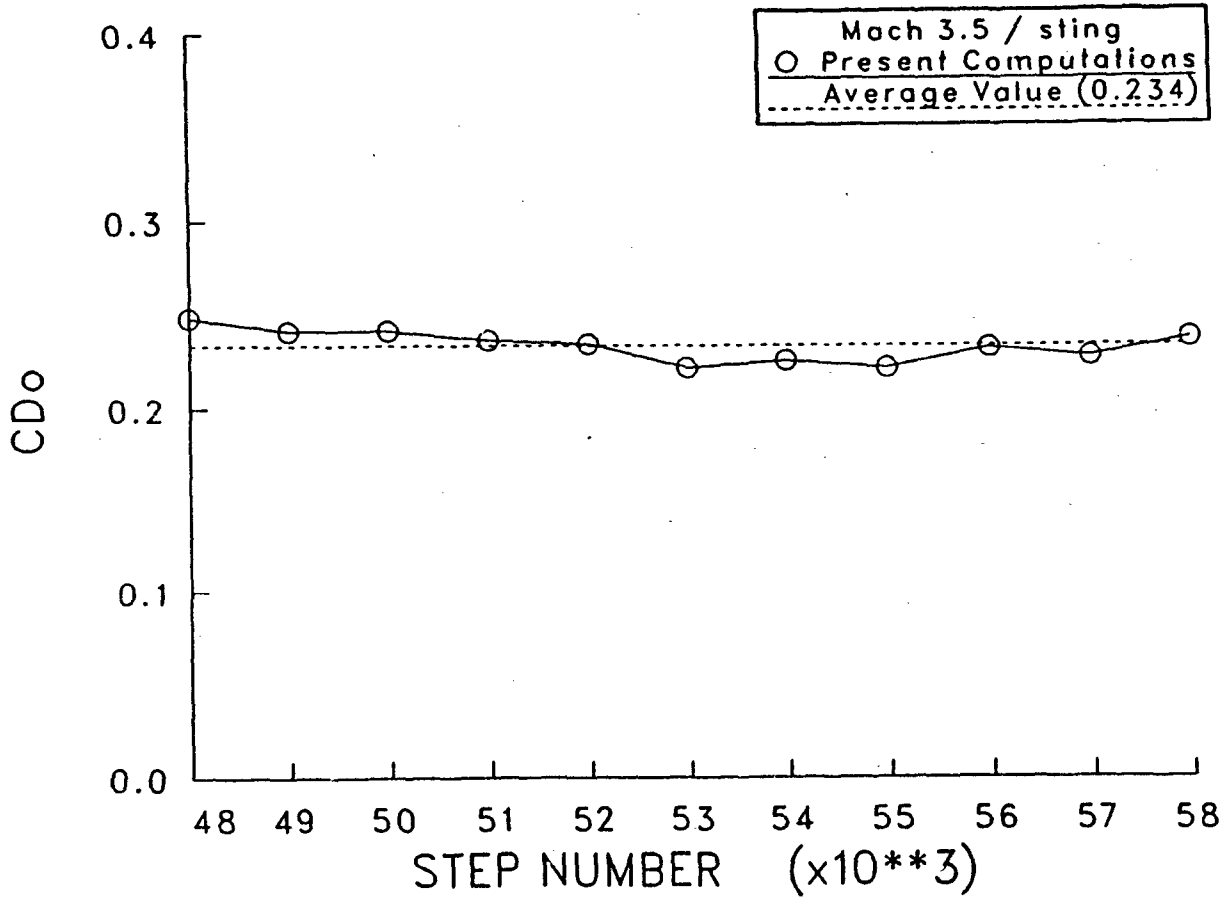

Figure 18. Numerical conversion history for M = 3.5 case

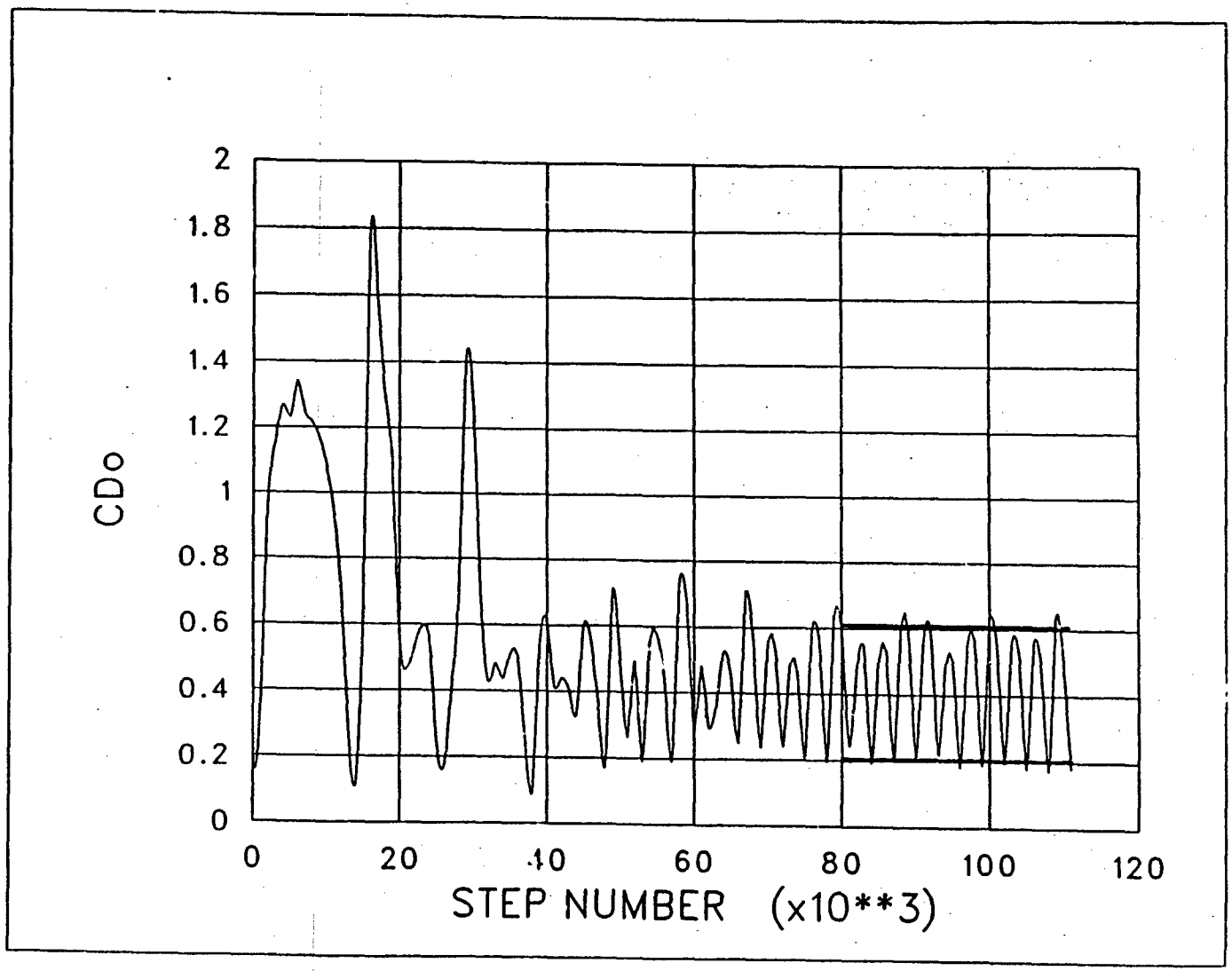

Figure 19. Oscillatory drag coefficient for the M = 1.9 case

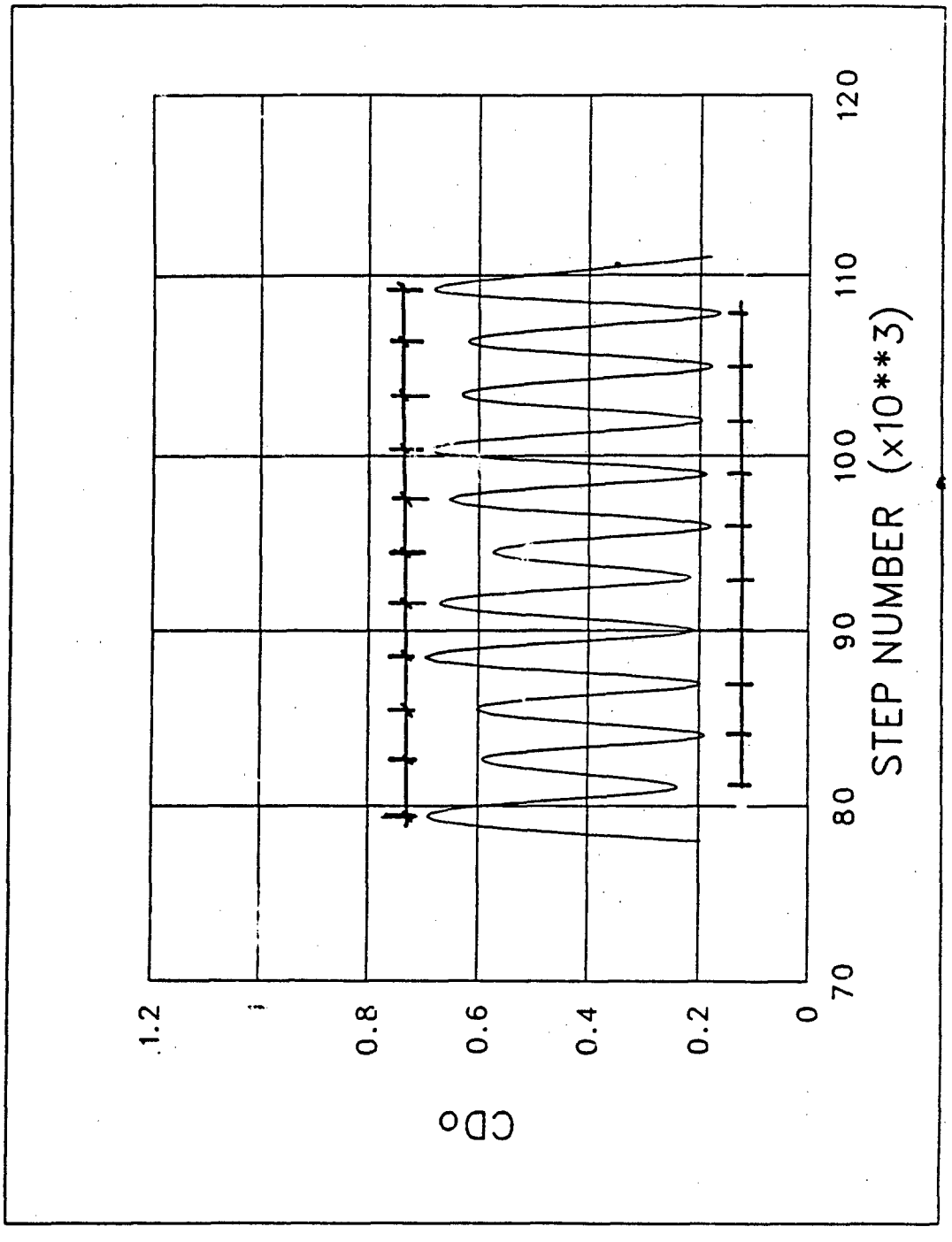

Figure 20. Oscillatory cycle for the M = 1.9 case

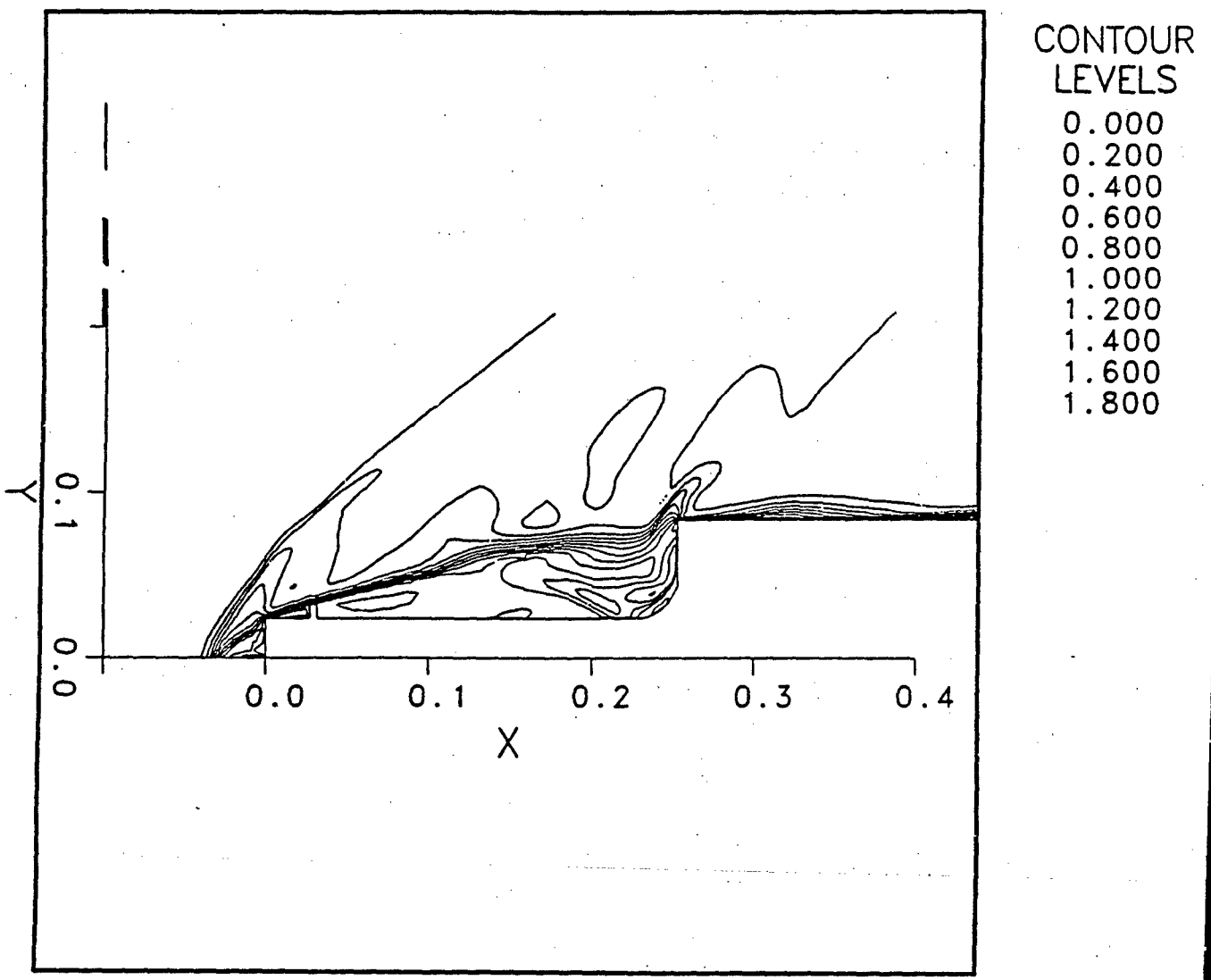

Figure 21. Flow field for the M = 1.9 case - near the spike tip, at high pressure point

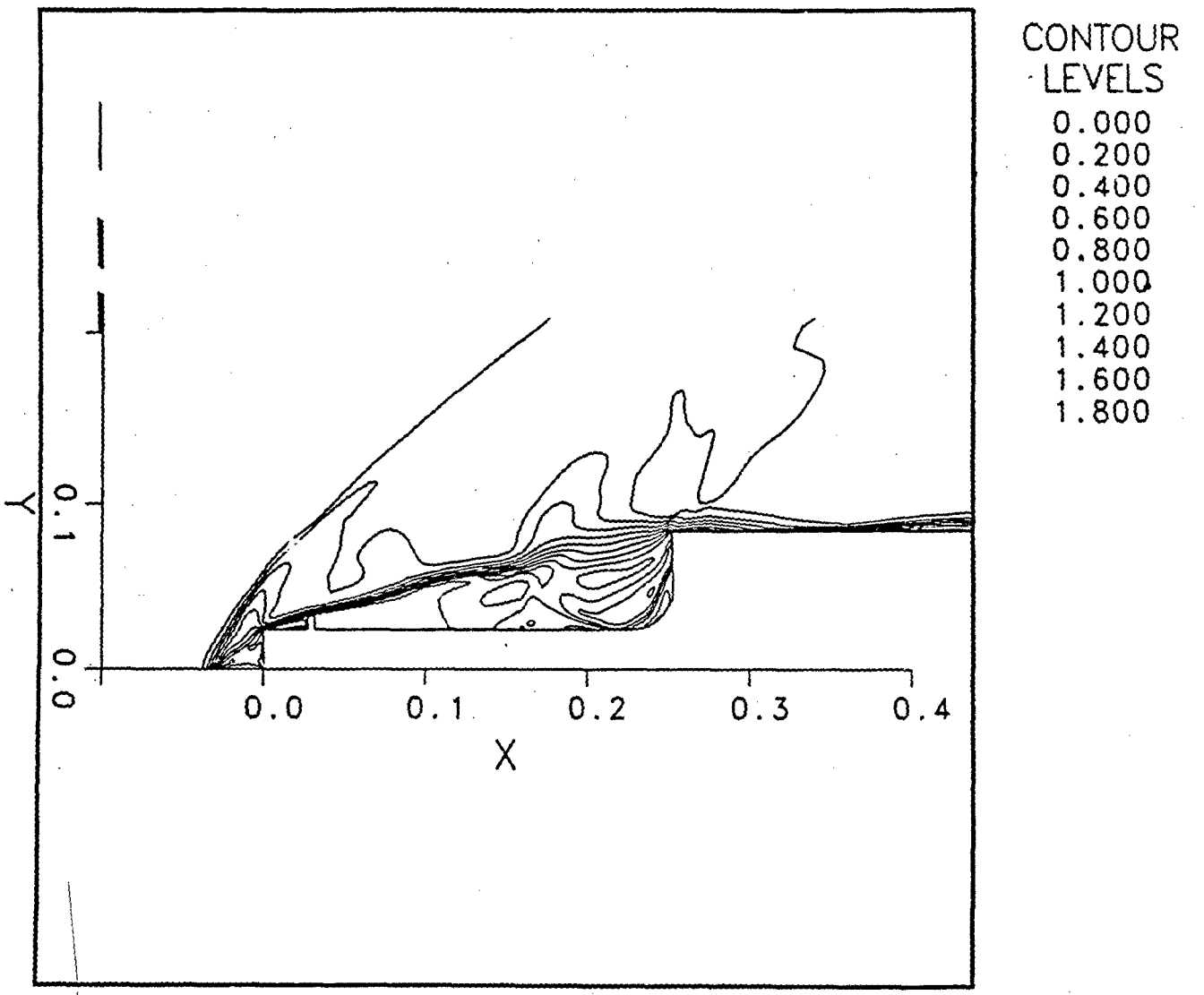

Figure 22. Flow field for the M = 1.9 case - near the spike tip, at low pressure point

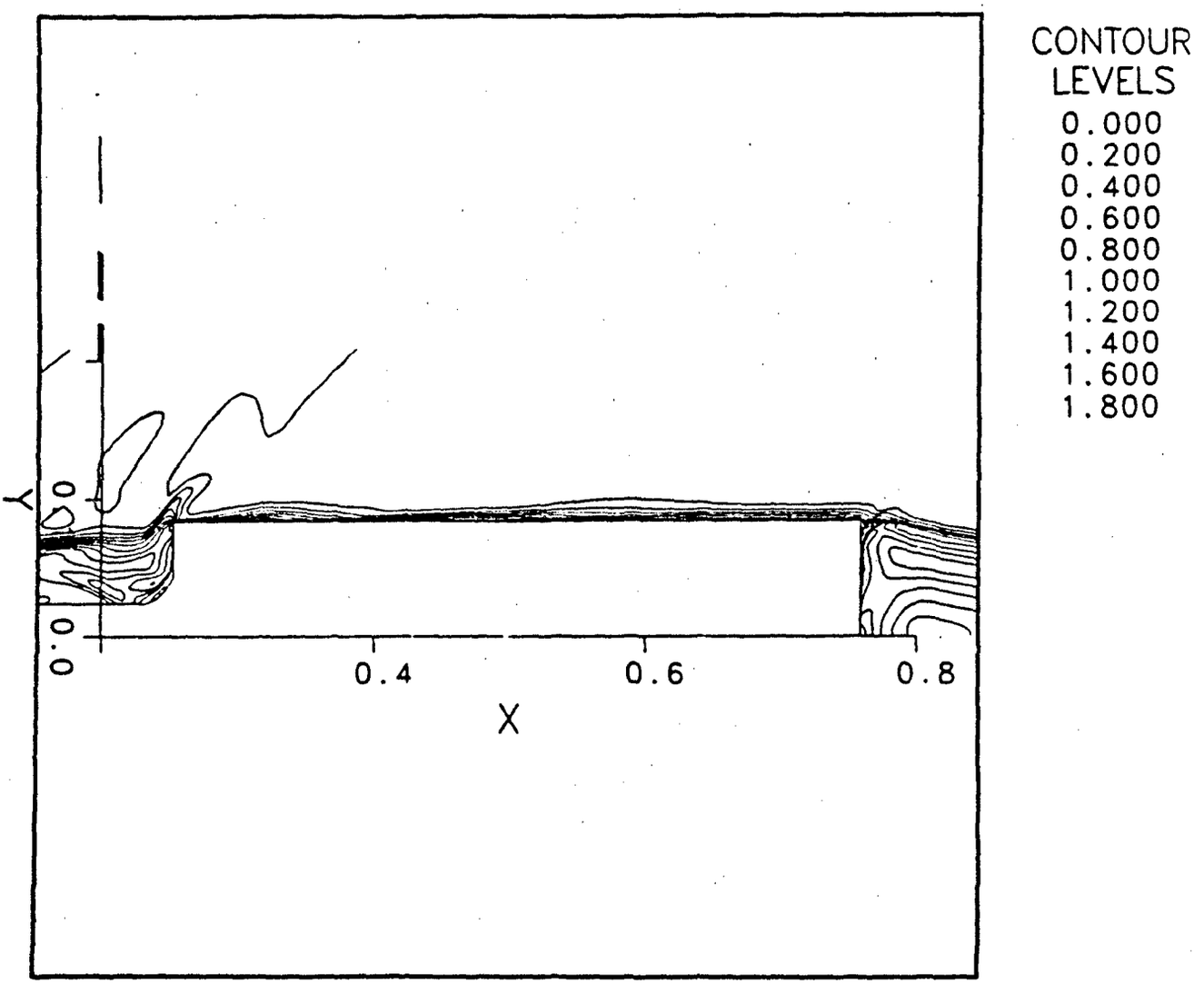

Figure 23. Flow field for the M = 1.9 case - near the shoulder, at high pressure point

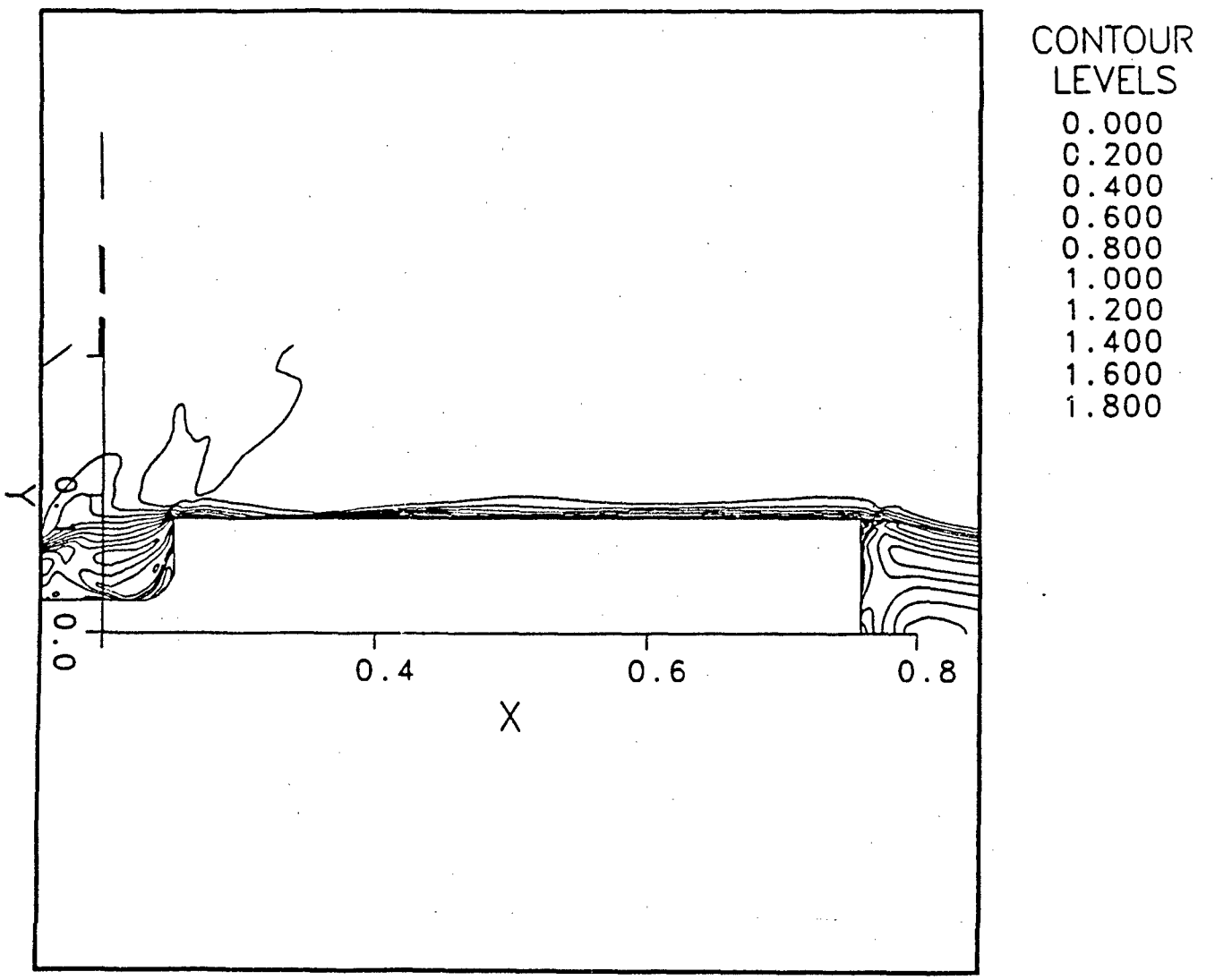

Figure 24. Flow field for the M = 1.9 case - near the shoulder, at low pressure point

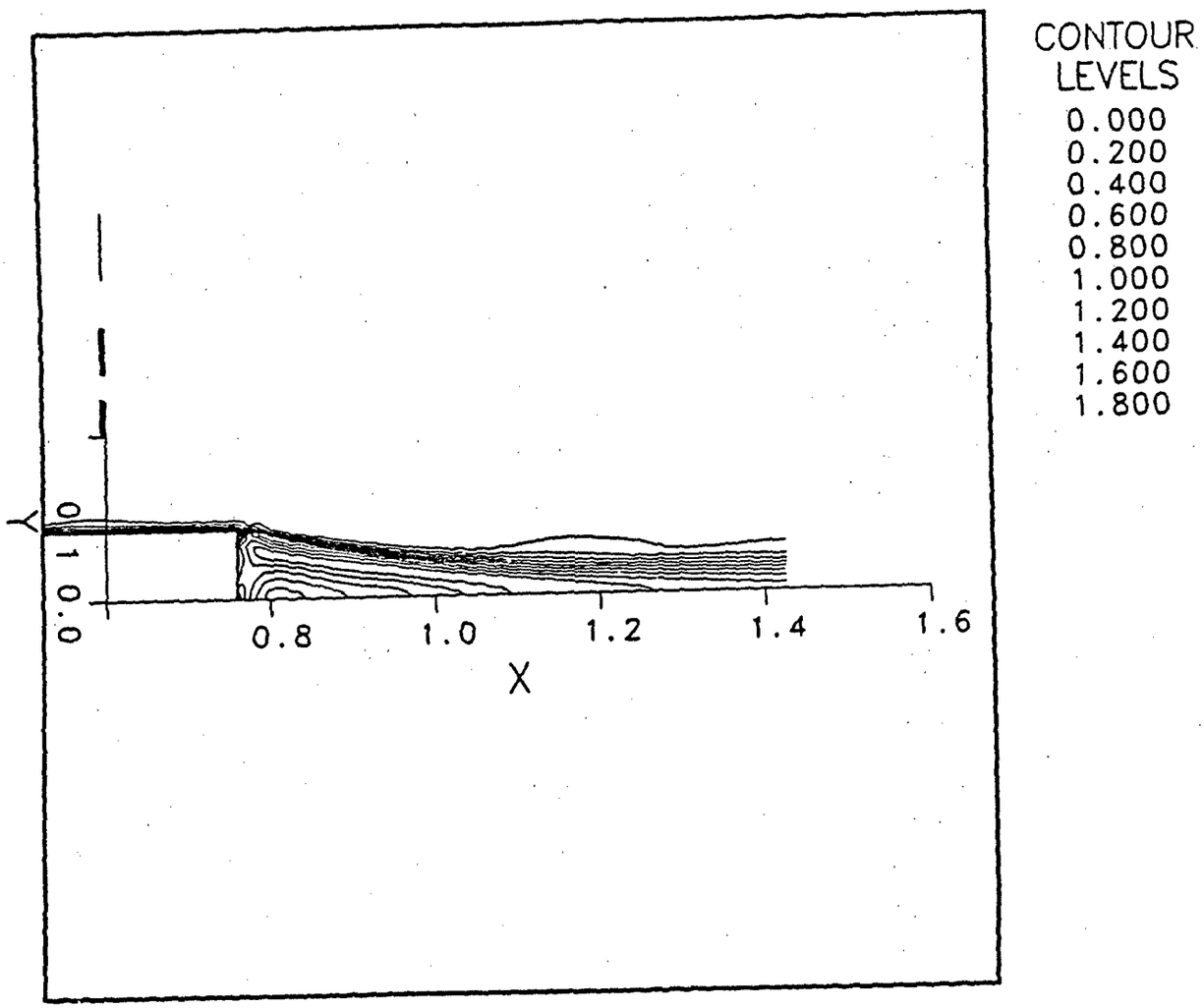

Figure 25. Flow field for the M = 1.9 case - near the base, at high pressure point

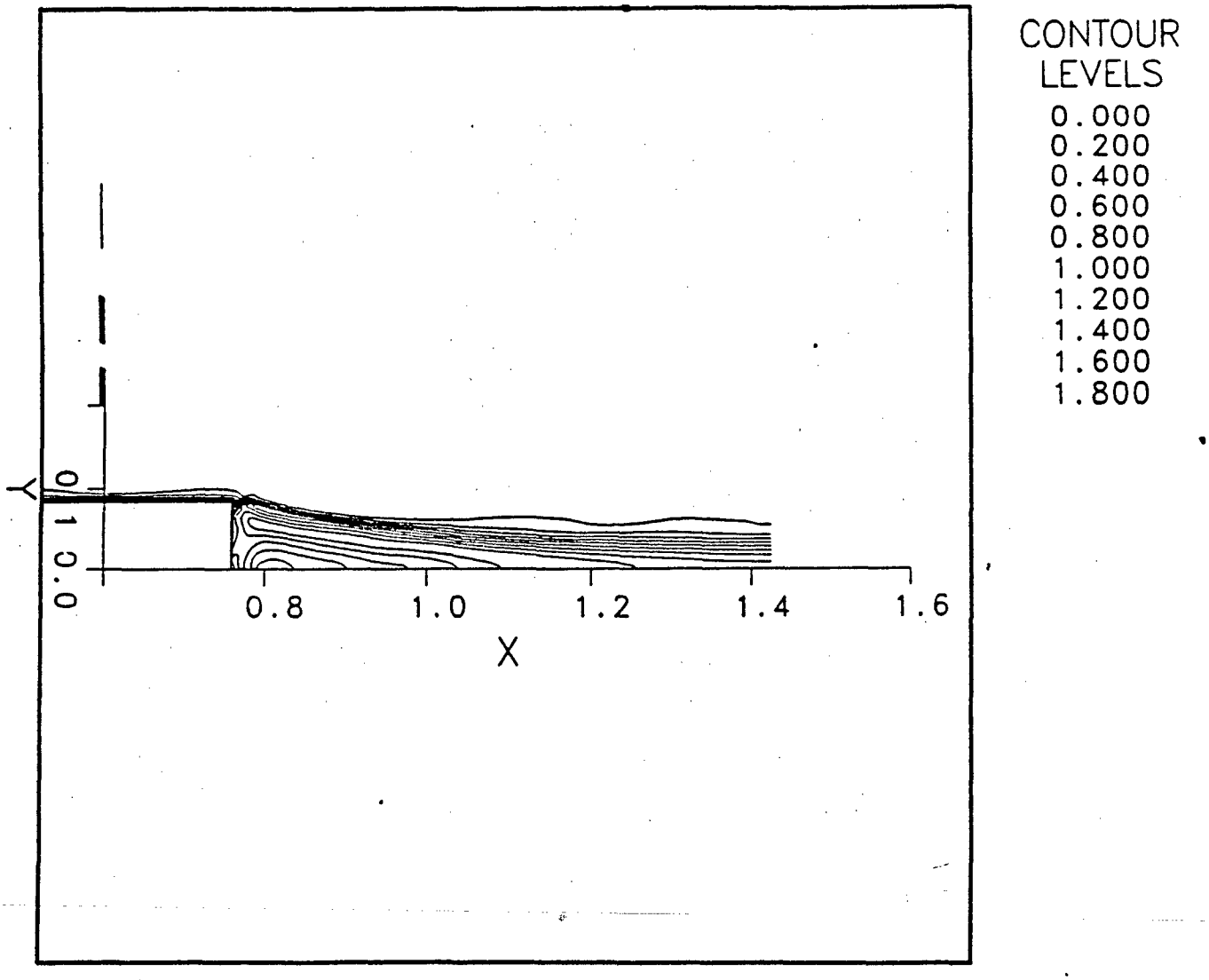

Figure 26. Flow field for the M = 1.9 case - near the base, at low pressure point

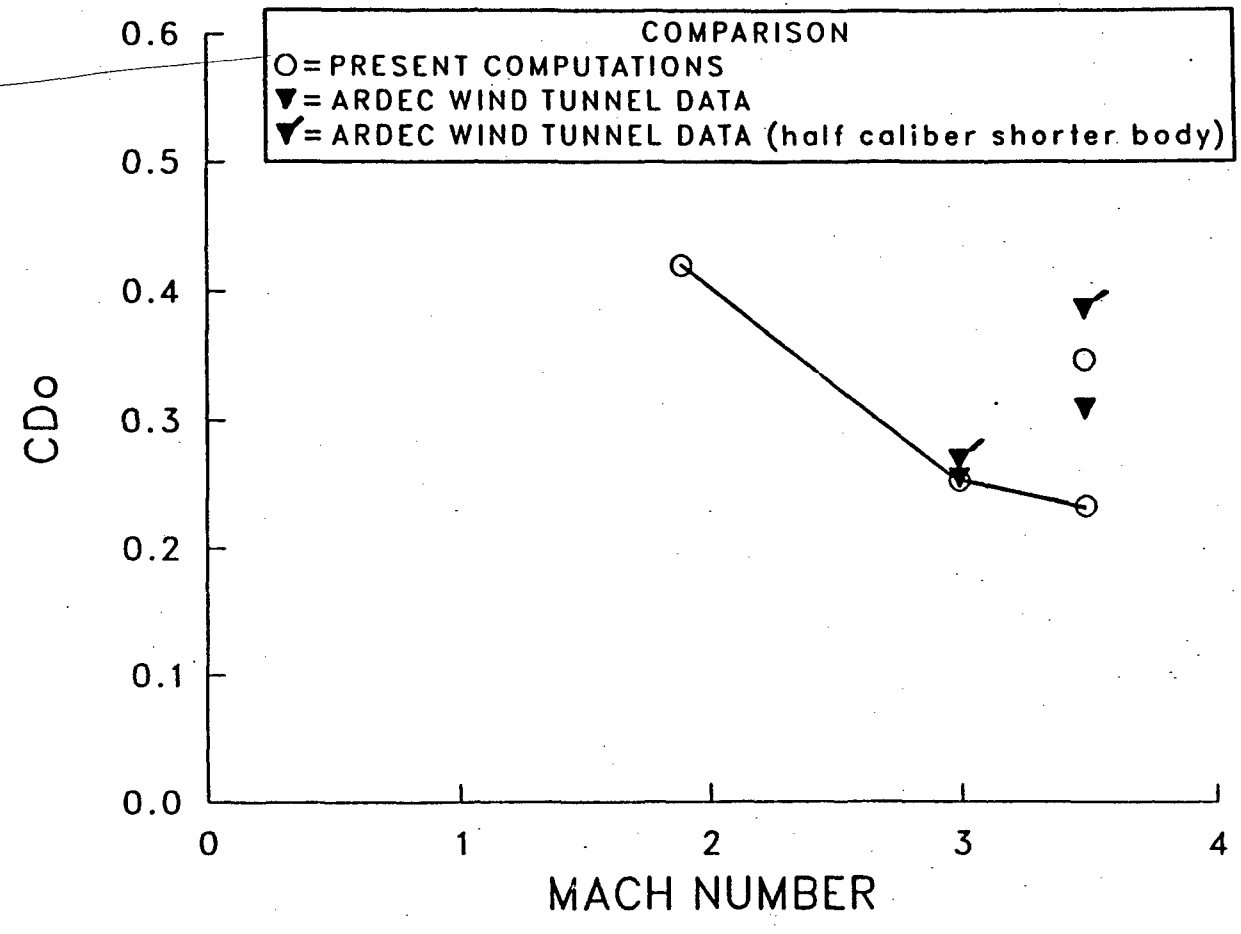

Figure 27. Drag coefficient comparison for all cases computed

INTENTIONALLY LEFT BLANK.

References

1. Platou, A.S., "Body Nose Shapes for Obtaining High Static Stability," BRL-MR-592, U.S. Army Ballistic Research Laboratory, Aberdeen Proving Ground, Maryland, February 1952.

2. Koenig, K., Bridges, D.H., and Chapman, G.T., "Transonic Flow Modes of an Axisymmetric Blunt Body," AIAA Paper No. 88-3536, 1st National Fluid Dynamics Congress, Cincinnati, Ohio, July 1988.

3. Shang, J.S., Hankey, W.L., and Smith, R.E., "Flow Oscillations of Spike-Tipped Bodies," AIAA Journal, Vol. 20, No. 1, January 1982, pp. 25-26.

4. Calarese, W. and Hankey, W.L., "Modes of Shock-Wave Oscillations on Spike-Tipped Bodies," AIAA Journal, Vol. 23, No. 2, February 1985, pp. 185-192.

5. Mikhail, A.G., "Spike-Nosed Projectiles: Computations and Dual Flow Modes in Supersonic Flight," BRL-TR-3140, U.S. Army Ballistic Research Laboratory, Aberdeen Proving Ground, Maryland, August 1990. (also Journal of Spacecraft and Rockets, Vol. 28, No. 4, July-August 1991,pp. 418-424.)

6. Falkowski, E.W. and Fleming, G.C., "Aerodynamic Characteristics of the Modified 105-mm M490 Training Projectile," Technical Report ARLCD-TR-81043, U.S. Army Large Caliber Weapon Systems Labratory, Dover, New Jersey, April 1982.

7. Unpublished Firing Range Measurements, Launch and Flight Division, U.S. Army Ballistic Research Laboratory, Aberdeen Proving Ground, Maryland, 1980.

8. Patel, N.R. and Sturek, W.B., "Multi-Tasked Numerical Simulation of Axisymmetric Ramjet Flows Using Zonal Overlapped Grids," BRL-MR-3834, U.S. Army Ballistic Research Laboratory, Aberdeen Proving Ground, Maryland, May 1990.

9. Baldwin, B.S. and Lomax, H., "Thin-Layer Approximation and Algebraic Model for Separated Turbulent Flows," AIAA Paper No. 78-257, January 1978.

10. Danberg, J.E. and Patel, N.R., "An Algebraic Turbulent Model For Flow Separation Caused by Forward and Backward Facing Steps," BRL-MR-3791, U.S. Army Ballistic Research Laboratory, Aberdeen Proving Ground, Maryland, December 1989.

11. Jou, W-H. and Menon, S., "Large Eddy Simulation of Flow in Ramjet Combustor," 22nd JANNAF Combustion Meeting Proceeding, CPIA Publication 432, Vol. I, Chemical Propultion Information Agency, Silver Spring, Maryland, October 1985, pp. 331-339.

INTENTIONALLY LEFT BLANK.

LIST OF SYMBOLS

A_{ref}	= reference area, $(\pi d^2/4)$
C_D	= drag coefficient, drag force/$(0.5\rho V^2 A_{ref})$
C_p	= specific heat under constant pressure
C_v	= specific heat under constant volume
d	= reference diameter
ds	= spike diameter
e	= specific total energy
J	= Jacobian of the coordinate transformation
M	= Mach number
p	= static pressure
Re	= Reynolds number
T	= temperature
u, v	= velocity components in the x, y directions
V_∞	= free stream velocity
x, y	= Cartesian coordinates for 2-D case, axial and radial coordinates for axisymmetric case

Greek Symbols

α	= angle of attack
γ	= ratio of specific heats
ρ	= density
μ	= laminar (molecular) viscosity coefficient
ϵ	= turbulent eddy viscosity coefficient
ξ, η	= transformed coordinates in the computational plane for the coordinates x, y

Subscripts

o	= denotes total (stagnation) condition
∞	= free stream condition

INTENTIONALLY LEFT BLANK.

No. of Copies	Organization
2	Administrator Defense Technical Info Center ATTN: DTIC-DDA Cameron Station Alexandria, VA 22304-6145
1	Commander U.S. Army Materiel Command ATTN: AMCAM 5001 Eisenhower Ave. Alexandria, VA 22333-0001
1	Director U.S. Army Research Laboratory ATTN: AMSRL-D 2800 Powder Mill Rd. Adelphi, MD 20783-1145
1	Director U.S. Army Research Laboratory ATTN: AMSRL-OP-CI-AD, Tech Publishing 2800 Powder Mill Rd. Adelphi, MD 20783-1145
2	Commander U.S. Army Armament Research, Development, and Engineering Center ATTN: SMCAR-IMI-I Picatinny Arsenal, NJ 07806-5000
2	Commander U.S. Army Armament Research, Development, and Engineering Center ATTN: SMCAR-TDC Picatinny Arsenal, NJ 07806-5000
1	Director Benet Weapons Laboratory U.S. Army Armament Research, Development, and Engineering Center ATTN: SMCAR-CCB-TL Watervliet, NY 12189-4050
(Unclass. only) 1	Commander U.S. Army Rock Island Arsenal ATTN: SMCRI-IMC-RT/Technical Library Rock Island, IL 61299-5000
1	Director U.S. Army Aviation Research and Technology Activity ATTN: SAVRT-R (Library) M/S 219-3 Ames Research Center Moffett Field, CA 94035-1000

No. of Copies	Organization
1	Commander U.S. Army Missile Command ATTN: AMSMI-RD-CS-R (DOC) Redstone Arsenal, AL 35898-5010
1	Commander U.S. Army Tank-Automotive Command ATTN: ASQNC-TAC-DIT (Technical Information Center) Warren, MI 48397-5000
1	Director U.S. Army TRADOC Analysis Command ATTN: ATRC-WSR White Sands Missile Range, NM 88002-5502
1	Commandant U.S. Army Field Artillery School ATTN: ATSF-CSI Ft. Sill, OK 73503-5000
(Class. only) 1	Commandant U.S. Army Infantry School ATTN: ATSH-CD (Security Mgr.) Fort Benning, GA 31905-5660
(Unclass. only) 1	Commandant U.S. Army Infantry School ATTN: ATSH-CD-CSO-OR Fort Benning, GA 31905-5660
1	WL/MNOI Eglin AFB, FL 32542-5000
	Aberdeen Proving Ground
2	Dir, USAMSAA ATTN: AMXSY-D AMXSY-MP, H. Cohen
1	Cdr, USATECOM ATTN: AMSTE-TC
1	Dir, ERDEC ATTN: SCBRD-RT
1	Cdr, CBDA ATTN: AMSCB-CI
1	Dir, USARL ATTN: AMSRL-SL-I
10	Dir, USARL ATTN: AMSRL-OP-CI-B (Tech Lib)

No. of Copies	Organization
4	Commander U.S. Army Armament Research, Development, and Engineering Center ATTN: SMCAR-FSP-A, Kline Grau Kahn Hudgins Picatinny Arsenal, NJ 07806-5000
2	Commander Dahlgren Division Naval Surface Warfare Center ATTN: Code DK20, Clare Moore Dahlgren, VA 22448-5000
1	Commander Naval Surface Warfare Center Applied Mathematics Branch ATTN: Code R44, Dr. A. Wardlaw White Oak Laboratory Silver Spring, MD 20903-5000
1	Director NASA Ames Research Center ATTN: MS N227-8, L. Schiff Moffett Field, CA 94035
2	Director Sandia National Laboratories ATTN: Dr. W. Oberkampf Dr. F. Blottner Division 1636 P.O. Box 5800 Albuquerque, NM 87185
1	Commander U.S. Army Missile Command ATTN: Dr. W. Walker Redstone Arsenal, AL 35898-5241
1	Massachusetts Institute of Technology ATTN: Tech Library 77 Massachusetts Ave. Cambridge, MA 02139

No. of Copies	Organization
1	Director Defense Advanced Research Projects Agency ATTN: Tactical Technology Office 3701 North Fairfax Dr. Arlington, VA 22203-1714
2	Southwest Research Institute ATTN: Mr. T. R. Jeter Dr. R. White Energetics Systems P.O. Box 28510 San Antonio, TX 78284
1	Battelle Northwest ATTN: Mr. M. Garnich P.O. Box 999 Richland, WA 99358
1	Lockheed Company ATTN: Mr. John Gerky P.O. Box 33, Dept. 1/330 Ontario, CA 91761
1	United States Military Academy Department of Civil and Mechanical Engineering ATTN: LTC Andrew L. Dull West Point, NY 10996
1	AAI Corporation ATTN: Dr. T. Stastney P.O. Box 126 Hunt Valley, MD 21030-0126

USER EVALUATION SHEET/CHANGE OF ADDRESS

This Laboratory undertakes a continuing effort to improve the quality of the reports it publishes. Your comments/answers to the items/questions below will aid us in our efforts.

1. ARL Report Number ARL-TR-101 Date of Report March 1993

2. Date Report Received _____

3. Does this report satisfy a need? (Comment on purpose, related project, or other area of interest for which the report will be used.) _____

4. Specifically, how is the report being used? (Information source, design data, procedure, source of ideas, etc.) _____

5. Has the information in this report led to any quantitative savings as far as man-hours or dollars saved, operating costs avoided, or efficiencies achieved, etc? If so, please elaborate. _____

6. General Comments. What do you think should be changed to improve future reports? (Indicate changes to organization, technical content, format, etc.) _____

CURRENT ADDRESS

_____
Organization

_____
Name

_____
Street or P.O. Box No.

_____
City, State, Zip Code

7. If indicating a Change of Address or Address Correction, please provide the Current or Correct address above and the Old or Incorrect address below.

OLD ADDRESS

_____
Organization

_____
Name

_____
Street or P.O. Box No.

_____
City, State, Zip Code

(Remove this sheet, fold as indicated, staple or tape closed, and mail.)

DEPARTMENT OF THE ARMY

OFFICIAL BUSINESS

BUSINESS REPLY MAIL
FIRST CLASS PERMIT No 0001, APG, MD

Postage will be paid by addressee

Director
U.S. Army Research Laboratory
ATTN: AMSRL-OP-CI-B (Tech Lib)
Aberdeen Proving Ground, MD 21005-5066

NO POSTAGE
NECESSARY
IF MAILED
IN THE
UNITED STATES